COMPARATIVE SEISMIC PERFORMANCE ASSESSMENT OF CONTINUOUS SLAB ON GIRDER BRIDGES WITH MULTI COLUMN PIER BENT AND HAMMERHEAD PIER FOR SOFT AND STIFF SOIL CONDITIONS

A THESIS SUBMITTED TO
THE GRADUATE SCHOOL OF NATURAL AND APPLIED SCIENCES
OF
MIDDLE EAST TECHNICAL UNIVERSITY

BY

ÇAĞRI İMAMOĞLU

IN PARTIAL FULFILLMENT OF THE REQUIREMENTS
FOR
THE DEGREE OF MASTER OF SCIENCE
IN
ENGINEERING SCIENCES

FEBRUARY 2018

ABSTRACT

COMPARATIVE SEISMIC ASSESSMENT OF CONTINUOUS SLAB ON GIRDER BRIDGES WITH MULTI COLUMN PIER BENT AND HAMMERHEAD PIER FOR SOFT AND STIFF SOIL CONDITIONS

İmamoğlu, Çağrı
MSc. Department of Engineering Sciences
Supervisor: Prof. Dr. Murat Dicleli

February 2018, 76 pages

This thesis is mainly focused on comparative seismic assessment of bridges with multi-colum pier bent and hammerhead pier under soft to stiff soil conditions. Soil and structure interaction (SSI) plays a vital role in bridge engineering as SSI on buildings and SSI on bridges. Moreover, bridges with tall piers having high aspect ratios are chosen in order to investigate the effects of rocking. The scope of this thesis is limited to symmetrical bridges having high aspect ratios. SSI in bridges is taken into consideration. In order to examine the interaction between soil and bridge, soil is modelled by three types of springs which work for sliding, rocking and shear of the foundation as well as force-displacement relationships of backfill including radiation damping. These springs are taken from Beam on Nonlinear Winkler Foundation Model. After modelling the soil, bridge models are chosen from real life in order to observe the effects of soil and structure interaction realistically. The analyses are conducted under loose, medium dense and dense sand.

Keywords: Soil and Structure Interaction, Hammerhead, Multiple Column, Radiation Damping

ÖZ

ÇEKİÇ BAŞLI VE ÇOK KOLONLU ORTA AYAĞA SAHİP KİRİŞ-ÜZERİNE-TABLİYELİ SÜREKLİ KÖPRÜLERİN YUMUŞAK VE SERT ZEMİNLERDE SİSMİK PERFORMANSININ KARŞILAŞTIRMALI DEĞERLENDİRMESİ

İmamoğlu, Çağrı
Yüksek Lisans, Mühendislik Bilimleri Bölümü
Tez Yöneticis: Prof. Dr. Murat Dicleli

Şubat 2018, 76 sayfa

Bu tez çalışmasında çoklu kolona sahip köprü ayaklarıyla çekiç başlı köprü ayaklarının sismik etki altındaki davranışlarının hesaplamalı ve karşılaştırmalı analizi göz önünde bulundurulmuştur. Yapı ve zemin etkileşimi köprü mühendisliğinde önemli bir role sahiptir. Yapılarda ve zeminde, yapı-zemin etkileşimi olarak incelenebilir. Özellikle yüksek ayaklı köprüler seçilerek, yapının zemine saplanma etkisi incelenmeye çalışılmıştır. Tezin araştırma alanı, yüksek kesit alanine sahip ortaayaklardan oluşan simetrik köprülerle sınırlandırılmıştır. Köprü-zemin etkileşimini inceleyebilmek adına, zemin üç ayrı tip yay ile modellenmiştir. Bu yaylar, zeminin kayma, saplanma ve kesme kuvvetlerini modelleyecek şekilde dizayn edilmiştir. Sismik etkinin sönümlenmesi ve kenarayağın arkasında yer alan dolgu toprağın kuvvet-deplasman ilişkisi ayrıca modellenmiştir. Modellemede kullanılan bu yaylar, "Beam on Nonlinear Winkler Foundation" isimli modelden alınarak geliştirilmiştir. Toprağın modellenmesinin ardından ,gerçekte var olan köprüler, analiz için kullanılmıştır. Bu sayede, modellemenin gerçekçi olması amaçlanmıştır. Analizler, sert, orta-sert ve yumuşak kum üzerinde gerçekleştirilmiştir.

Anahtar Kelimeler: Toprak ve Yapı Etkileşimi, Çekiç başlı ortaayaklar, Çoklu kolona sahip ortaayaklar, Sönümleme

To my parents

ACKNOWLEDGEMENTS

This MSc thesis could not have been completed without the great support I have received from my parents and my closest friends. It is a great pleasure for me to thank every single of them.

First, I would like to thank my supervisor, Prof Dr Murat Dicleli, an irreplaceable member of Department of Engineering Sciences, Middle East Technical University for his unconditional support, guidance, inspiration, valuable ideas and feedbacks over the years. Whenever I struggled to solve problems in numerous fields of my thesis studies, he came up with solutions which show his experience and skills in engineering.

Secondly, I would like to thank Assoc. Prof. Dr. Mustafa Tolga Yılmaz. His knowledge on foundation engineering helped me in order to understand the soil and structure interaction in earnest.

Secondly, I would like to thank Dr. Ali Salem Milani, a superb member of Department of Engineering Sciences. His knowledge of structural engineering and his great personality helped me significantly throughout my thesis study.

I would especially like to thank for my friends Türköz Gargun, Bikem Bennu Baksı, Simay Seyrek, Ahmet Özdemir and Çağdaş Demirkan who supported me in those hard times. Without their support, it would be almost impossible for me to achieve my goal in my thesis studies.

Last but not least, I would like to thank for my mum and grandma who supported me throughout my life, starting from the day I was born.

To the people, whom I have forgotten to mention their names to thank for, I would have to owe an apology.

TABLE OF CONTENTS

LIST OF TABLES

LIST OF FIGURES

CHAPTER 1

INTRODUCTION

Soil and structure interaction (SSI) plays a major role in order to model the structure realistically. SSI could be divided into two divisions as SSI on buildings and SSI on bridges. SSI in bridges could be divided into three branches. These are abutment-backfill interaction, soil-pile interaction and foundation-soil interaction. This thesis mainly focuses on bridges with tall piers having high aspect ratios to investigate the effects of rocking. Since the effects of rocking are aimed to be modelled for shallow foundations and high piers, the effects of sliding are neglected due to the high ratio of pier height to footing length. Specifically, when the ratio of pier height to footing length becomes less than 1, sliding dominates the behaviour (Gajan, Kutter, 2009). But this ratio is much higher in the examples considered in the thesis. The scope of this thesis is limited to symmetrical bridges having high aspect ratios. For shallow foundations, rocking effect is important. In order to understand the effects of rocking, the SSI mechanism is investigated due to the nonlinear behaviour of soil. This nonlinearity may cause settlement, rotation and sliding. (Gajan, Kutter, 2005) After the observations made in soil-structure interaction field, it is understood that the subject of soil-structure interaction has to be examined in earnest. Therefore, it is focused on to create a model in order to illustrate the effects of cyclic loadings on shallow foundations.

The thesis has two main objectives which are:

- First objective is to study rocking on the seismic response of the bridges.
- Second objective is to understand the relationship between rotation and moment of the foundation in order to simulate the behaviour of the foundation and hysteresis effects.

The research mainly focuses on comparative seismic assessment of two bridge pier types as multi-column pier bent and hammerhead pier for stiff and soil conditions on shallow foundations. First, an extensive literature review is conducted. Secondly, soil-structure interaction behaviour of shallow foundations is explained. Following this explanation, the bridges and parameters used in this thesis are determined. Following this determination, the bridges are designed and modelled. After designing and modelling the bridges, the results are analysed. Then, these analyses are discussed. Finally, the conclusion is made. In the following sections, these steps are explained in a detailed fashion.

An extensive literature review is conducted on the historical background of soil-structure interaction, soil-structure interaction modelling and soil-structure interaction analyses. Based on this information, the necessity of this thesis is introduced. The information obtained from this literature review is used in order to model the rocking shallow foundations under cyclic loadings.

Gajan, Kutter, Hutchinson et al. (2007) modelled the shallow foundation under cyclic loadings by the use of BNWF (Beam on Nonlinear Winkler Foundation) springs. These springs are used to define the loading, unloading and reloading phases of the cyclic loading. This model is considered to be the most complete model since it defines all phases of loading.

To use the moment-rotation backbone curve obtained in Phase 2, BNWF springs have to be examined in earnest. In this chapter, these springs are introduced and the properties of them are given. These springs are used to model the medium dense and dense soil. There are three types of springs which model the soil according to their densities. Since the structure can undergo displacement in three ways, namely as in vertical direction and horizontal directions, the springs are specialized to model the soil-foundation interaction under these three circumstances. In this chapter, the details of these springs are given.

After completing the “Soil-Footing Interaction” Chapter, the bridges are chosen to be modelled by SAP2000. These bridges are chosen according to their pier types, span lengths and width of piers.

The design of the bridges is performed in compliance with AASHTO (2014). In order to complete the design phase, earthquake excitations are chosen from PEER Ground Motion Database.

Following the design of the bridges, the models of the bridges are created by the aid of the program in SAP2000. This program is used in order to create the model by considering various aspects of bridge modelling.

After creating the models of the bridges, the cyclic loadings are applied to the bridge models. The analyses are obtained from SAP2000.

After analysing the models, the results are discussed in earnest.

The conclusion is made by comparing the seismic performance assessment of continuous slab on girder bridges with multi-column pier bent and hammerhead pier for medium dense and dense soil conditions.

CHAPTER 2

LITERATURE REVIEW

Soil-structure interaction (SSI) is an interdisciplinary field. It is completely linked with other disciplines as structural mechanics, earthquake engineering and soil dynamics. This discipline was discovered in late 19th century and it developed in the beginning of the 20th century. But major developments were made in the second half of the 20th century thanks to the powerful computers and programs. These developments are introduced chronologically as follows:

The very first major development was made by Erich Reisner in 1936. He explored the behaviour of circular discs on elastic half-spaces subjected to time-harmonic vertical loads. But this exploration did not manage to succeed since he assumed in his theory that the plate considered in his study had frictionless contact with the soil. In 1937, he focused on contact shearing stresses which increased linearly with distance to the axis. Other than Reisner, Sagoci, Apsel, Luco, Veletsos, Wei and Westmann helped the field to show progression.

In the beginning of 1970s, Veletsos, Luco and Westmann made the invaluable contribution to the field. The studies of them supplied solutions to the problem of circular plates underlain by elastic half-spaces excited dynamically over a wide range of frequencies. After this stage, the needs of nuclear power and offshore industries shaped the future of soil-structure interaction field.

From the mid-1960s to mid-1970s the powerful computers led the engineers to work on irregularly shaped foundations embedded in inhomogeneous or layered media. These developments evolved rapidly with the existence of the programs such as SHAKE, LUSH, SASSI and CLASSI in this era. In 1978 a heavyweight

in SSI field, Dominguez, obtained the impedances of rectangular foundations embedded in an elastic half space. (Kausel, 2009)

In the beginning of 2000s, the studies got narrowed down due to the specific industrial needs. The path of SSI field which is going to be followed in the future entirely relies on the needs of these necessities. All in all, today's conjecture shapes the future of this interdisciplinary field.

Soil-structure interaction has an extreme importance to simulate the seismic response of bridges. Rocking shallow foundations are considered to be advantageous over fixed-base foundations since they can absorb some of the ductility demands which would be absorbed by columns. It is observed that foundations designed for elastic behaviour cannot have these benefits of nonlinear soil-structure interaction (SSI). Furthermore, it is concluded that bridge systems with rocking foundations on good soil conditions show small settlements and good performance (Deng, Kutter, Kunnath, 2012). Moreover, shallow foundations might be loaded into their nonlinear range during major earthquake loadings. The nonlinearity of soil might act as an energy dissipation mechanism and it reduces the shaking demands which are exerted on the buildings. But if this nonlinearity is not considered, it might cause permanent deformations and damage to the building (Gajan, Kutter, Phalen et al., 2004). In case of soil yielding or foundation uplifting, the safety margins of the entire structure may increase but permanent displacement and rotation might occur which is totally undesirable (Kokkali, Abdoun, Anastasopoulos, 2015). Actually, bridge engineers generally depend on the performance of previously constructed bridges in which the soil-structure interaction (SSI) is not taken into account. Last but not least, today's design codes discourage designs which allow rocking. (Raychowdhury, Hutchinson, 2008)

The models considered in this section take soil-structure interaction modelling into account. The studies mentioned here consist of models which give

correlative results with the corresponding experimental data. However, these studies do not involve a full cycle which combines both moment-rotation backbone curves and hysteresis rules in harmony except one. Gajan, Kutter, Hutchinson et. al (2006) introduced the BNWF (beam on nonlinear Winkler foundation) springs which model the soil under loading, unloading and reloading phases. This model is used in the thesis. The details of this model is introduced to the reader in the following chapter.

One of the biggest problems considered in soil-foundation interaction is rocking. If the aspect ratio, which is" ", is smaller than 1, sliding dominates the behaviour (Gajan, Kutter, 2009). But since the models considered in the thesis have aspect ratios much larger than 1, rocking dominates the behaviour. Ugalde, Kutter, Jeremic et al. (2007) mentioned the effects of rocking in order to attract engineers' attention on rocking. The most important effect of rocking is, rocking results in lengthening of the natural period that tends to reduce acceleration and force demands and increase displacement demands on the superstructure. Based on an entirely different approach, Gajan and Kutter (2009) modelled shallow foundations subjected to combined cyclic loading. Rocking shallow foundation model was created by the use of Contact Interface Model (CIM) and the results of this model showed perfect correlation with the experimental data (p. 9). Raychowdhury and Hutchinson (2008) created a model to capture the sliding, settling and rocking movements of a shallow foundation when it was subjected to earthquake ground motions. This model was developed by the use of Beam-on-Nonlinear-Winkler-Foundation (BNWF) model which consisted of a system of uncoupled springs. These springs had nonlinear inelastic behavioural response. It was stated that, if the amplitude of rocking was acceptable, the energy sourced by earthquake excitations could be dissipated through soil-foundation interface with moment-rotation action. The theoretical results were in very good agreement with the experimental data. Harden, Hutchinson, Martin et.al (2005) created a numerical model of the nonlinear cyclic response of shallow foundations. That study was focused on the nonlinear behaviour of

shallow building foundations under large-amplitude loading. The model was based on performance-based earthquake engineering (PBEE). To use PBEE in a current design, BNWF model was chosen. The experimental results were compared with theoretical results and they were in very good agreement. Gajan, Kutter and Thomas (2005) conducted six series of tests in order to study nonlinear load-deformation characteristics of shallow foundations during cyclic loading. This nonlinearity was caused by progressive rounding of soil. This led to a reduction in contact area between footing and soil. Hence, contact element model was used in this study. Experimental data and the model were compared and the results were observed to be in very good agreement. Anastasopoulos, Gelagoti, Kourkoulis et al. (2011) developed a simplified model for the analysis of the cyclic response of shallow foundations. This study is at the forefront due to its simplified approach. It was based on the kinematic hardening constitutive model of Von Mises failure criterion and encoded in ABAQUS. The results were compared with the experimental data and the results were in very good agreement.

The studies were carried out on ordinary bridges under earthquake loads with an entirely new approach called direct displacement-based design (DDBD). A multilinear model was developed which represented the moment-rotation backbone curve of the nonlinear moment-rotation behaviour. In addition, an empirical relationship was proposed that correlated the initial stiffness to the moment capacity of a rocking foundation. In the design procedure Deng, Kutter and Kunnath (2014) constructed a bridge system which consisted of a deck mass, a rocking foundation and a damped elastic column integrated into a single element. By the use of this model, equivalent linear damping and period could be determined. DDBD used the equivalent system damping and period along with a design displacement response spectrum. The results were compared with theoretical data and it was observed that DDBD produced precise displacement values.

Up to now, the studies considered here captured the moment-rotation backbone curves by using CIM, BNWF, PBEE and DDBD. The results obtained here show good correlation with the experimental data. Specifically, the BNWF model is considered to be the used in the thesis since the unloading and reloading phases are defined explicitly and thoroughly.

Following the investigation of models which are based on soil-structure interaction modelling, soil-structure interaction analyses are examined in this section. The importance of nonlinear soil behaviour was examined and shown by conducting studies for structures with a constant base and variable height. Specifically, the importance of SSI increased when soil softens. (Kim, Y., Roesset, J.M., 2004). Seismic performance verifications for shallow foundations were generally assumed to be satisfied but it was understood that the shallow foundations are generally over-designed (Jiro, F., Masahiro S., Yoshinori, N., Ryuichi, A., 2005).

The general consensus is, the increasing number of cycles increases the residual displacement and stiffness degradation but the moment capacity is not affected significantly. The common point of the studies considered in this section is, none of them has a complete hysteresis curve which combines both the moment-rotation backbone curve and hysteresis rules. In order to understand the importance of rocking effect on shallow foundations, an extensive literature review is conducted as follows:

The analyses were done in various aspects. The effect of contact area ratio was examined by Gajan and Kutter (2008). The studies included several centrifuge experiments in order to study the rocking behaviour of shallow footings supported by sand and clay stratums. The tests were conducted during both slow cyclic loading and dynamic shaking.

The importance of soil-structure interaction was not only investigated on foundation basis. The effects of SSI were investigated on multi-span simply supported bridges. In order to examine these effects, FHWA's guidelines for footing foundation on semi-infinite elastic half space were used to determine translational and rotational stiffnesses at the base of bridge abutments and piers. It was concluded that SSI had a detrimental effect specifically on abutments rather than on the column piers. SSI affected plastic rotation demand and this demand was higher for medium dense soils rather than soft or stiff soils (Saadeghvaziri, M.A., Yazdani-Motlagh, A.R., Rashidi, S., 2000).

As it is discussed in section 1.4.1, today's conjecture shapes the future of SSI. In this regard, to evaluate the earthquake excitations on the seismic design of a nuclear containment structure, SSI was examined. The effects were observed by conducting several centrifuge tests on various soil conditions from loose sand to weathered rock. Subsoil condition, earthquake intensity and control motion affected the seismic design of nuclear power plants. It was concluded that soft soils (sandy and weathered soil) generate less amplification in soil layer and the period was lengthened more in soft soils compared to rock conditions (Ha, J., Kim, D., 2014)

Besides these studies mentioned in this section, kinematic responses of shallow foundations were studied and the results were tabulated. Based on these results, it was observed that coupling impedances were considered to be negligible for shallow foundations. (Mylonakis, G., Nikolaou, S., Gazetas, G., 2006)

Nonlinear behaviour of soil under seismic excitations were examined in various aspects by conducting 1G large-scale shake table test and cyclic eccentric loading tests. These aspects varied in loading methods, input seismic motions, soil densities and the ratio of horizontal and overturning moment loads. This set of data supplied information related to the model which examined the coupling effect of horizontal, vertical and overturning loads, the accumulation of residual

displacement and the foundation uplift. It was concluded that residual displacement was dependent on number of loading cycles, the coupling effect of vertical and horizontal displacement. More importantly, the uplift effect significantly affected the foundation behaviour in three aspects. These were the shape of the hysteresis loop, the degradation in rotational stiffness and the elongation of the vibration property (Shirato, M., Kouno, T., Asai, R. et al., 2008). Large-scale specimens of sand were constructed and tested under the cyclic loading imposed on a different shallow foundation model in order to improve the bearing capacity of soil-foundation systems. The tests were conducted with medium dense and dense sand examples. The results indicated that during uplift, the stiffness of the system degraded significantly but as soon as the eccentric load decreased, the contact area of the soil-foundation system increased and rocking stiffness recovered (Negro, P., Paolucci, R., Pedretti, S., Faccioli E. 2000).

The effects of cyclic loading on rocking shallow foundations were examined in earnest with increasing numbers of tests. The type of loadings, pier heights, soil densities were varied and the results were obtained. According to these results, when the shallow foundation was subjected to cyclic loading, the residual displacement accumulated with residual rotation and the final residual displacement was entirely dependent on numbers of cycles, loading patterns and soil densities (Jiro, F., Masahiro, S., Yoshinori, N., Ryuichi, A., 2005).

Another aspect of rocking shallow foundations was considered under cyclic loadings. Since it was aimed to ensure that rocking was materialized through uplifting rather than sinking, a large vertical factor of safety (FSv) was required but since the soil properties could not be foreseen, this application was considered to be feasible in theory. Since rocking-induced soil yielding was only mobilized within a shallow layer underneath the footing, “shallow soil improvement” was considered to eliminate the risks of unforeseen inadequate FSv. It was ensured that, with aspect ratios larger than 1, rocking dominated

sliding in the experiments. It was concluded in these series of tests that if the depth of the foundation was equal to the width of the foundation, shallow soil improvement could be effective. Last but not least, it was stated that increasing numbers of cycles alter the effectiveness of shallow soil improvement (Anastasopoulos, I., Kourkoulis, R., Gelagoti, R., et al. 2012).

The studies mentioned above, take soil-structure interaction into account in the modelling phase. But as mentioned in this section, BNWF springs are considered to be the most complete model in the design phase. Gajan, Hutchinson, Kutter et al. (2007) explained the properties of BNWF model. This model is considered to be the most complete model since it explains the elastic and plastic behaviour of soil in loading, unloading and reloading phases. Moreover, horizontal and vertical displacement of soil are taken into account in the same model.

CHAPTER 3

DESCRIPTION OF THE BRIDGES USED IN THE ANALYSES

In this chapter, description of the bridges is introduced to the reader. The reasons why Eskişehir Köseköy Bridge is used in the analyses are explained in earnest.

In order to compare the seismic effects on continuous slab on girder bridges with multi-column pier bent and hammerhead pier, the bridges constructed in real life are examined. KMG, Inpro and Yuksel Project played a significant role in this part of the thesis since these three firms supplied the bridges constructed according to the research field of the thesis.

The survey mentioned in "Choice of Bridges" consists of 44 bridges. 13 of these bridges have multi-column head piers and 31 of them have hammerhead piers. They are designed for 0.3g-0.4g peak ground acceleration. The survey includes prestressed and post-tensioned bridges. These bridges are mainly categorized under two branches according to their pier types which are multi-column pier bent and hammerhead pier. The related aspect ratios of these piers in both lateral and transverse directions are tabulated. Furthermore, to model these bridges realistically, same study is carried out for the left and right abutments of these bridges.

In tables 3.1, 3.2, 3.3 and 3.4, the aspect ratios of the bridges in this study are taken into consideration.

Table 3.1. Aspect Ratio Results of Multi-Column Pier Bent (h/B)

ASPECT RATIO RESULTS (h/B)			
MAX	MIN	AVERAGE	ST DEV
1.669	0.567	1.185	0.241

Table 3.2. Aspect Ratio Results of Multi-Column Pier Bent (h/L)

ASPECT RATIO RESULTS (h/L)			
MAX	MIN	AVERAGE	ST DEV
3.000	0.311	1.078	0.860

Table 3.3. Statistical Results of the Distribution of the Aspect Ratios(h/B)

(h/B)	# of data	AR	%
0.5-1.0(0.756)	3	0.756	10.71
1.0-1.5(1.202)	24	1.102	85.71
1.5-2.0(1.624)	2	1.624	7.14

Table 3.4. Statistical Results of the Distribution of the Aspect Ratios(h/L)

(h/L)	# of data	AR	%
0-0.5(0.445)	13	0.44	46.43
0.5-1.0(0.721)	7	0.721	25.00
1.0-1.5(1.25)	1	1.25	3.57
1.5-2.0(1.833)	1	1.833	3.57
2.0-2.5(2.302)	4	2.302	14.29
2.5-3.0(2.597)	2	2.597	7.14
3.0-3.5(3.000)	1	3	3.57

The values in parenthesis under “h/B” and “h/L” columns indicate the average values of aspect ratios in their current range. For instance, 3 samples of h/B data have an aspect ratio, varying in between 0.5 and 1.0. The average of these three samples equals 0.756. Here, “B” stands for the breadth of the foundation and “L” stands for the length of the foundation.

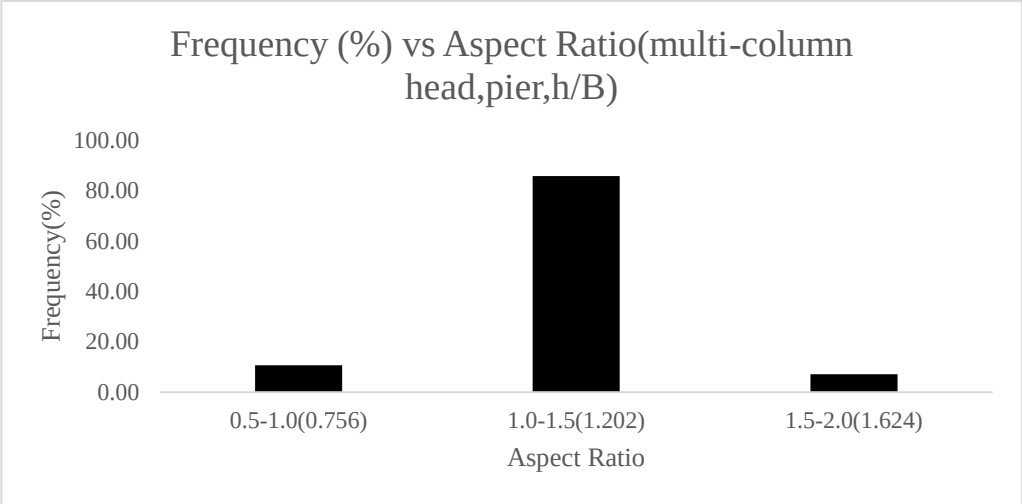

Figure 1. Frequency vs Aspect Ratios of Multi-Column Pier Bent (h/B)

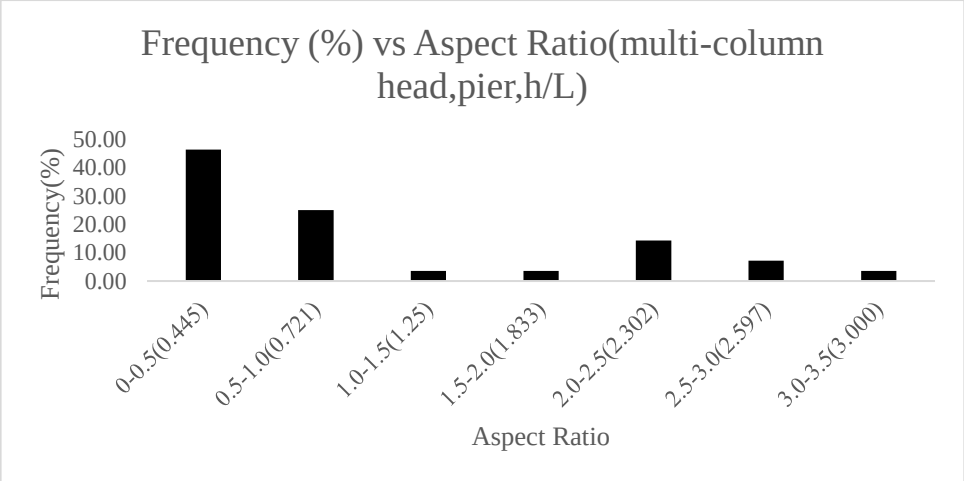

Figure 2. Frequency vs Aspect Ratios of Multi-Column Pier Bent (h/L)

Table 3.5. Aspect Ratio Results of Hammerhead Pier (h/B)

ASPECT RATIO RESULTS (h/B)			
MAX	MIN	AVERAGE	ST DEV
3.800	0.442	1.663	0.604

Table 3.6. Aspect Ratio Results of Hammerhead Pier (h/L)

ASPECT RATIO RESULTS (h/L)			
MAX	MIN	AVERAGE	ST DEV
3.470	0.447	1.514	0.589

Table 3.7. Statistical Results of the Distribution of the Aspect Ratios (h/B)

h/B	# of data	AR	%
0-0.5(0.442)	1	0.442	0.51
0.5-1.0(0.822)	26	0.822	13.33
1.0-1.5(1.231)	52	1.231	26.67
1.5-2.0(1.746)	63	1.746	32.31
2.0-2.5(2.194)	34	2.194	17.44
2.5-3.0(2.704)	15	2.704	7.69
3.0-3.5(3.045)	2	3.045	1.03
3.5-4.0(3.661)	2	3.661	1.03

Table 3.8. Statistical Results of the Distribution of the Aspect Ratios (h/L)

h/L	# of data	AR	%
0-0.5(0.472)	2	0.472	1.03
0.5-1.0(0.801)	40	0.801	20.51
1.0-1.5(1.226)	57	1.226	29.23
1.5-2.0(1.701)	52	1.701	26.67
2.0-2.5(2.221)	32	2.221	16.41
2.5-3.0(2.672)	11	2.672	5.64
3.0-3.5(3.47)	1	3.47	0.51

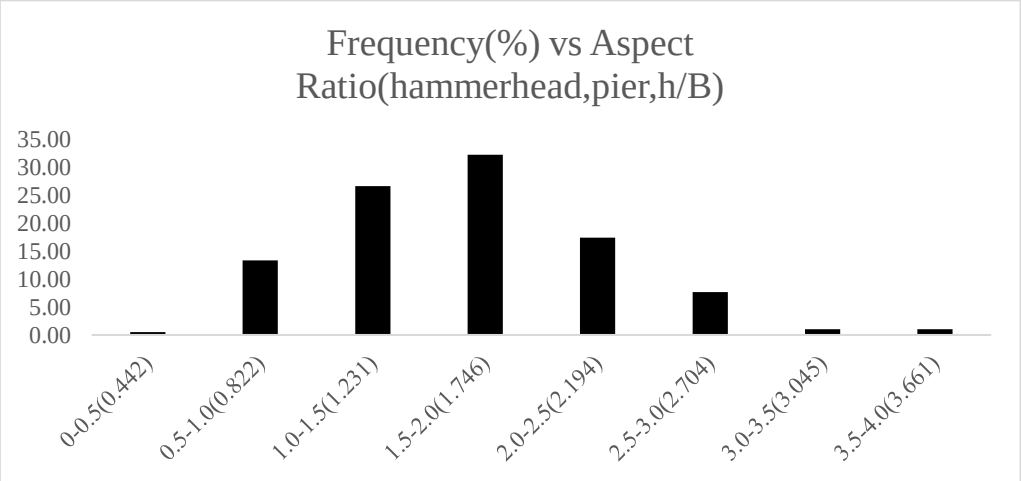

Figure 3. Frequency vs Aspect Ratios of Hammerhead Pier (h/B)

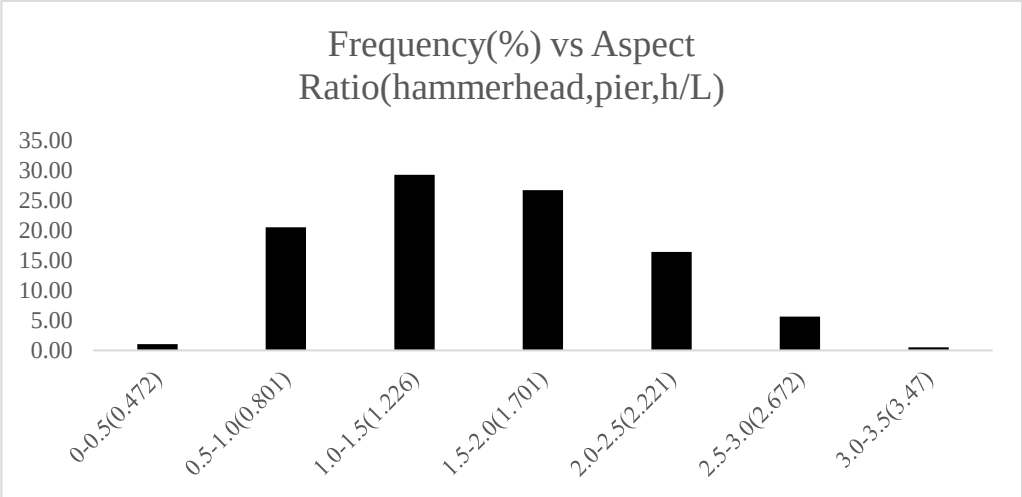

Figure 4. Frequency vs Aspect Ratios of Hammerhead Pier (h/L)

Under the light of these analyses, Eskişehir Köseköy Bridge is chosen for modelling. The aspect ratios of the piers of Eskişehir Köseköy Bridge in longitudinal direction are 1.619, 1.769 and 1.763. These results comprise of 32% of the total range as shown on the previous chart. Moreover, the aspect ratios of the same bridge in transverse direction are found as 1.295, 1.415 and 1.410. These results comprise of almost 27% of the total range as shown on the previous chart. Hence Eskişehir Köseköy Bridge is considered to be a common bridge in terms of its aspect ratios.

Eskişehir Köseköy Bridge has equal spans with 32 meters. In the thesis, three spans of this bridge are modelled including its abutment and the foundations of both abutment and piers. Since it is considered to model the bridge under earthquake excitation with dense, medium dense and loose sand, the foundations are designed by the coefficients of Meyerhof and Brinch-Hansen (Salgado, 2003).

Köseköy Bridge is a railway bridge. The width of this bridge is 12 meters. It has two lanes. Figures 5,6, and 7 give an overview related to the bridge considered in this study.

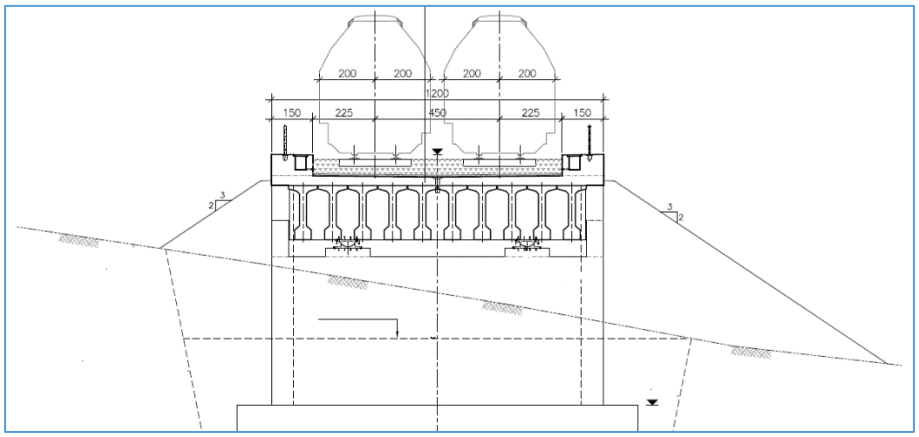

Figure 5. Cross Sectional View of Köseköy Bridge

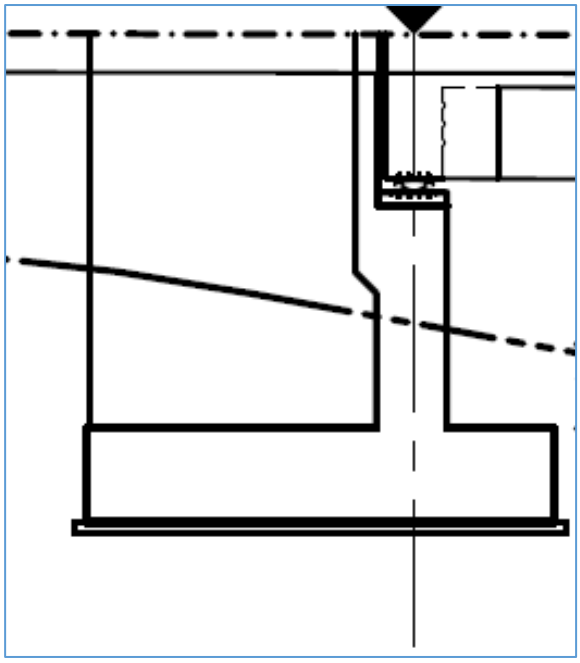

Figure 6. The Side View of the Abutment

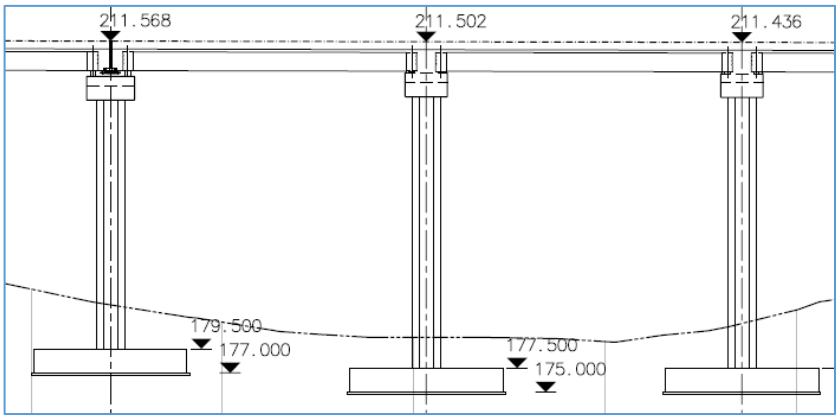

Figure 7. The Side View of the Bridge

CHAPTER 4

FOUNDATION SOIL PARAMETERS USED IN THE DESIGN FOR VARIOUS SOIL TYPES

In this chapter, the parameters used in the design for modelling the soil are introduced. After this introduction, the Beam on Nonlinear Winkler Foundation (BNWF) model is introduced.

Three types of soil stiffnesses are used in order to observe the effects of rocking.

Bowles (1997) classified the soil as very loose, loose, medium, dense and very dense. In this thesis, loose, medium and dense sand types are taken into consideration.

Table 4.1. . Properties of Sand Types Considered in This Study (Bowles,1997)

Description	Very Loose	Loose	Medium	Dense	Very Dense
Relative Density,D_r	0	0.15	0.35	0.65	0.85
Φ_{fine}	26-28	28-30	30-34	33-38	<50
Φ_{medium}	27-28	30-32	32-36	36-42	<50
Φ_{coarse}	28-30	30-34	33-40	40-50	<50
γ_{wet} (kN/m3)	11-16	14-18	17-20	17-22	20-23

Table 4.2. Soil Properties Used in This Study from FHWA (1997), AASHTO(2014) and Bowles (1997)

Soil Type	γ_1 (kN/m^3)	N_2	$G_{max(2)}$ (kPa)	$V_{s,(2)}$ (m/s)	AASHTO Soil Class$_{(3)}$
Dense Sand	20	40	224000	330	D
M. Dense Sand	18	18	118000	250	D
Loose Sand	16	7	55000	150	E

Density values are tabulated form Bowles (1997), shear modulus values and the shear wave velocities are tabulated from FHWA (1997) and soil classes are taken from AASHTO(2014).

After introducing the necessary parameters for the soil types considered in this thesis, BNWF Model is introduced as follows:

BNWF model is developed for a 2D-analysis. Hence 1D elastic beam column elements have 3 DoF's per node as horizontal, vertical and rotation. Individual 1D zero-length springs are independent of each other with nonlinear inelastic behavior modeled using modified versions of Qzsimple1, Pysimple1 and Tzsimple1.

Qzsimple1 simulates vertical load-displacement behavior. Pysimple1 simulates horizontal passive load-displacement behavior against the side of a footing and Tzsimple1 simulates the horizontal shear-sliding behavior at the base of the footing.

The schematic view below represents the locations of the springs. Vertical springs are distributed along the footing. Horizontal springs are located along both the short and long edge of the footing in order to capture shear and sliding behavior.

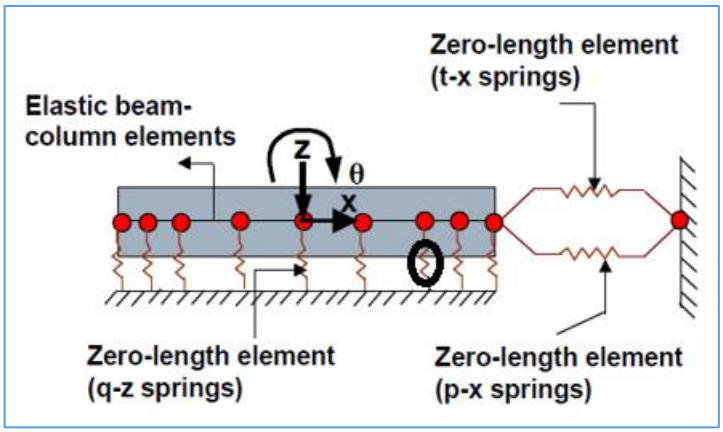

Figure 8. Beam on Nonlinear Winkler Foundation (BNWF) Schematic View

Furthermore the model mentioned above can capture hysteretic energy dissipation and account for radiation damping at the foundation base. All three types of springs are characterized by a nonlinear backbone curve, resembling a bilinear behavior. The bilinear curve consists of a linear and a nonlinear region with gradually decreasing stiffness as displacement increases. For Pysimple1 and Tzsimple1 springs, an ultimate load is defined for both tension and compression. Qzsimple1 springs have a reduced strength in tension to account for soil's limited tensile capacity. The working mechanism of the QzSimple1 material is explained in Figure 9. This material is spotted with a circle in Figure 8.

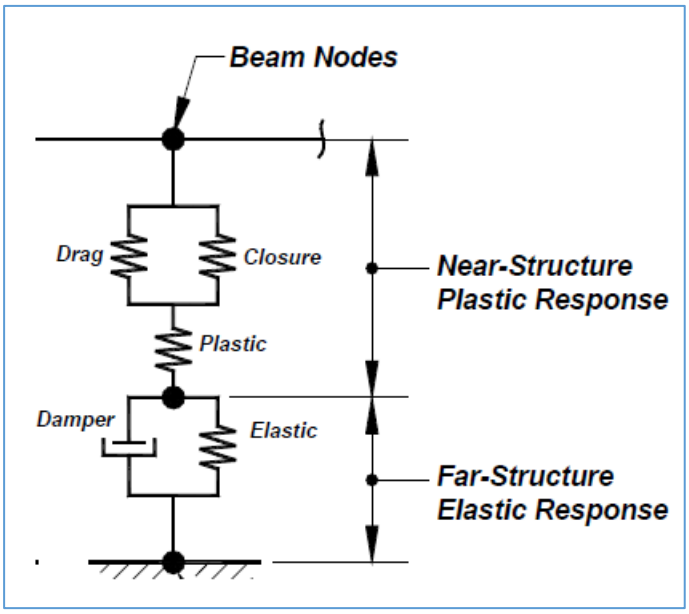

Figure 9. Typical zero length spring (proposed model)

Elastic and plastic components are added in series via gap elements in the proposed model created by Gajan, Kutter et al.(2008). The gap component of the spring is a parallel combination of a closure and a drag spring. The closure component is a bilinear elastic spring which is relatively rigid in compression and very flexible in tension. For shallow foundations, a single spring is used since the footing is assumed to be rigid with respect to shear and flexural deformations over its height.

The model considered in the thesis is more simplistic and gives realistic results. Instead of connecting the damper and elastic spring in parallel, every member is linked in series.

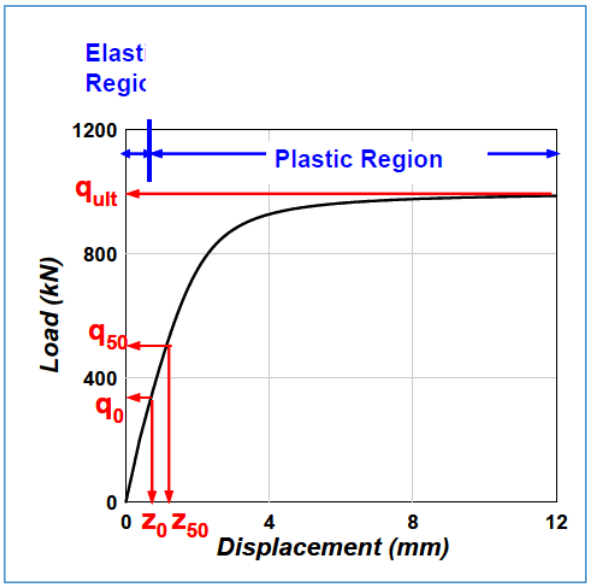

Figure 10. Nonlinear Backbone Curve for Qzsimple1 material

This backbone curve consists of two regions which are elastic region and inelastic region. The formulae which govern these regions are given as follows:

In the elastic region:

$$q = k_{in} z \tag{1}$$

$$q_0 = C_r q_{ult} \tag{2}$$

The elastic stiffness values are obtained from Gazetas (1991):

In vertical direction;

$$k_z = \frac{GL}{1-\nu}\left[0.73 + 1.54\left(\frac{B}{L}\right)^{0.75}\right] \tag{3}$$

In horizontal direction (toward long side of the footing);

$$k_y = \frac{GL}{2-\nu}\left[2 + 2.5\left(\frac{B}{L}\right)^{0.85}\right] \tag{4}$$

In horizontal direction (toward short side of the footing);

$$k_x = \frac{GL}{2-\nu}\left[2 + 2.5\left(\frac{B}{L}\right)^{0.85}\right] + \frac{GL}{0.75-\nu}\left[0.1\left(1 - \frac{B}{L}\right)\right] \tag{5}$$

The formula which holds true for the nonlinear region is given as follows:

$$q = q_{ult} - (q_{ult} - q_0)\left[\frac{cz_{50}}{cz_{50} + |z - z_0|}\right]^n \tag{6}$$

z_{50}: displacement where 50% of the total displacement is mobilized

z_0: displacement at the yield point

The equations derived above are valid for Qzsimple1, Pysimple1 and Tzsimple1 springs.

By the use of the equations mentioned above, the gapping capabilities of Qzsimple1 and Pysimple1 springs, the reduced tensile strength of Qzsimple1 spring and the hysteresis of the sliding resistance (without gapping) of Tzsimple1 spring are shown as follows:

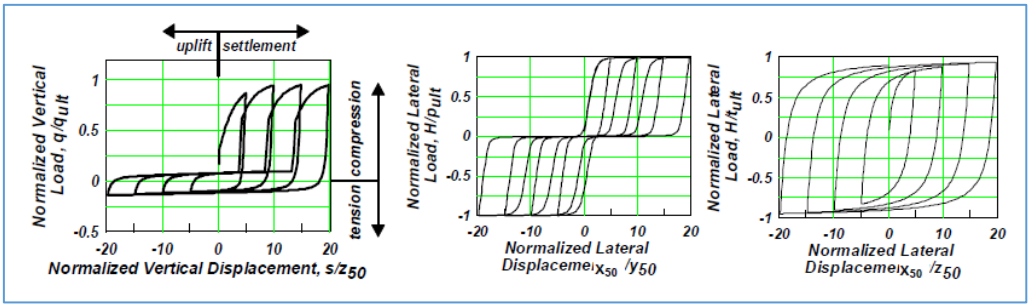

Figure 11. Cyclic response of uni-directional zero-length spring models: (a) axial load-displacement response, (b) lateral passive response (Pysimple1 material), (c) lateral sliding response (Tzsimple1 material)

The parameters given in equations (1), (2) and (3) have to be identified. Since sand is taken into consideration, the cohesion parameter, c is equal to zero whereas the internal angle of friction is not equal to 0.

In order to capture the behavior of Qzsimple1, Pysimple1 and Tzsimple1 springs, the following equations are derived as follows:

The ultimate bearing capacity of a $Q_{vertical}$ spring is given in equation (7).

$$q_{ult} = cN_cF_{cs}F_{cd}F_{ci} + \gamma D_f N_q F_{qs} F_{qd} F_{qi} + 0.5\gamma B N_\gamma F_{\gamma s} F_{\gamma d} F_{\gamma i} \qquad (7)$$

For sand, c equals zero which is the cohesive intercept. Hence the first part of the summation is cancelled out. The equations for each factor given in Equation (7) are derived by Salgado (2006):

It has to be stated that the parameters in equation (7), are used from both Meyerhof (2006) and Brinch-Hansen (2006).

γ: soil unit weight;

D_f: embedment;

$$N_q = \frac{1+sin\emptyset}{1-sin\emptyset} e^{\pi tan\emptyset} \quad (8)$$

N_q: bearing capacity factor for soil surcharge (unitless)

ϕ: friction angle;

$$F_{qs} = \left(1 + \frac{B}{L} \times sin\emptyset\right) \quad (9)$$

N: flow number;

$$N = \frac{1+sin\emptyset}{1-sin\emptyset} \quad (10)$$

$$If\ \frac{D}{B} \leq 1;\ F_{qd} = 1 + 2 \times tan\emptyset \times (1 - sin\emptyset)^2 \times \frac{D}{B} \quad (11)$$

$$If\ \frac{D}{B} > 1; F_{qd} = 1 + 2 \times tan\emptyset \times (1 - sin\emptyset)^2 \times tan^{-1}\frac{D}{B} \quad (12)$$

B: breadth, D: depth within a soil mass;

$$F_{qi} = \left[1 - \frac{arctan\left(\frac{Q_{tr}}{Q_{ax}}\right)}{90^0}\right]^2 \quad (13)$$

arctan(Q_{tr}/Q_{ax}): inclination angle of the load

$$N_\gamma = 1.5\left(N_q - 1\right)tan\emptyset \quad (14)$$

$$F_{\gamma s} = 1 - 0.4\frac{B}{L} \quad (15)$$

$$F_{\gamma d} = 1$$

N_γ: bearing capacity factor for unit weight term (unitless)

$$F_{\gamma i} = \left[1 - \frac{arctan\left(\frac{Q_{tr}}{Q_{ax}}\right)}{\emptyset}\right]^2 \quad (16)$$

The working mechanism of the spring which simulates the passive load-displacement behavior against a footing is given as follows:

$$p_{ult} = 0.5\gamma D_f^2 K_p \quad (17)$$

K_p: passive earth pressure coefficient. In this work, Coulomb's expression is used. That expression is given as follows:

$$K_p = \frac{sin^2(\beta - \emptyset)}{sin^2\beta sin(\beta+\delta)\left[1-\sqrt{\frac{sin(\emptyset+\delta)sin(\emptyset+\alpha)}{sin(\beta+\delta)sin(\beta+\alpha)}}\right]^2} \quad (18)$$

K_p can be expressed by Rankine's derivation. That derivation is more simplistic than Coulomb's expression which is mentioned below:

$$K_p = tan^2\left(45 + \frac{\emptyset}{2}\right) \quad (19)$$

The mechanism of springs which illustrate the shear-sliding behavior is given as:

$$t_{ult} = W_g tan\delta + A_b c \quad (20)$$

W_g: vertical force acting at the base of the foundation

δ: angle of friction between the foundation and soil (typically varying from $\frac{1}{3}\emptyset$ to $\frac{2}{3}\emptyset$).

A_b: area of the base of the footing in contact with the soil

c: cohesion intercept (It is zero for sand.)

After determining the formulae which govern the elastic and plastic regions of the springs, the end length ratio and the stiffness intensity ratio parameters are given as follows:

Stiffness Intensity Ratio, $R_k = \frac{k_{end}}{k_{mid}}$ (21)

End Length Ratio, $R_e = \frac{L_{end}}{L}$ (22)

L_{end}: length of the edge region over which the stiffness is increased. L_{end} is recommended as B/6 by ATC-40. This length can be determined from the following figure:

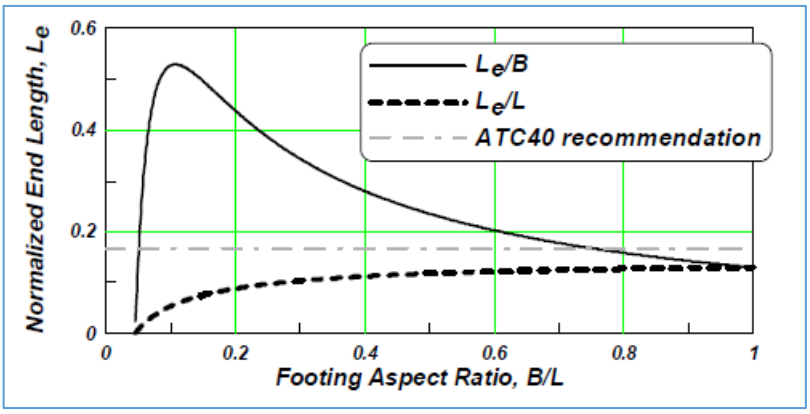

Figure 12. End length ratio versus footing aspect ratio

Stiffness Intensity Ratio can be determined from the following figure:

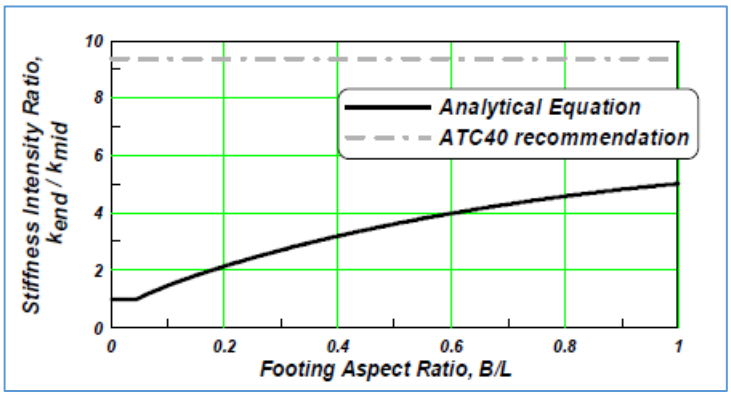

Figure 13. Stiffness intensity ratio versus footing aspect ratio

Spring spacing: $s = \frac{l_e}{L}$. Minimum number of 25 springs is recommended.

L: footing length

l_e: length of the footing element

Initial unloading stiffness is equal to initial loading stiffness.

The stiffness of the elastic range can be derived from Equation (1). It is defined by C_r. The stiffness of the plastic range can be derived from Equation (3) as follows:

$$k_p = n(q_{ult} - q_0)\left[\frac{(cz_{50})^n}{(cz_{50} - z_0 + z)^{n+1}}\right] \quad (23)$$

Following table shows the values of C_r, c and n which are constitutive parameters to determine the limits of elastic and plastic range:

Table 4.3. Nonuser defined parameters (Raychowdhury and Hutchinson, 2008)

Material Type	Soil Type	References	Values Used in the Current Study		
			Cr	n	c
QzSimple1	Sand	Vijayvergiya(1977)	0.36	5.5	9.29
PySimple1	Sand	API(1993)	0.33	2	1.1
TzSimple1	Sand	Mosher(1984)	0.48	0.85	0.26

Concluding Remarks:

- R_k (end stiffnes ratio) affects the permanent settlement significantly. On the other hand, its effect on maximum rotation and maximum stiffness is too slight.
- R_e (end length ratio) has a modest effect on the shape of the settlement-rotation and moment-rotation curve and nominally on total settlement.
- A smoother footing response occurs when a great number of springs are used.
- A larger C_r extends the elastic region, reduces the total settlement for a given load. A smaller C_r increases the total settlement.
- Constitutive parameter, c, affects the nonlinear portion of rotational stiffness and settlement significantly.
- Reducing the unloading stiffness to 20% of the loading stiffness, only increases the settlement by 6%.
- As mentioned above, the unloading load-displacement curve is identical in shape to the loading curve.

After the explanation of QzSimple1, PySimple1 and TzSimple1 materials, the nonlinear backbone curves of these materials are obtained. In this thesis, the names of these materials are changed in order to prevent confusion. The springs

which work vertically are labeled as $Q_{vertical}$. The springs which slide and shear are labeled as Q_{slide} and Q_{shear}, respectively.

The project consists of comparative seismic assessment of bridges under loose to stiff soil conditions. First, the spring properties of Eskişehir Köseköy Bridge are determined under dense soil conditions for $Q_{vertical}$, Q_{slide} and Q_{shear} materials. After determination of these properties, the same project is examined under medium dense conditions for these three materials. The parameters of these bridges considered in this study are given in the table as shown:

Table 4.4. Parameters of the bridges considered in this study

	Eskişehir Köseköy Bridge (under dense sand conditions)	Eskişehir Köseköy Bridge (under medium-dense sand conditions)	Eskişehir Köseköy Bridge (under loose sand conditions)
$\gamma(kN/m^3)$ (dense/medium dense)	20	18	16
D_f (m)	6	6	6
B (m)	10	11	11
L (m)	14	14	15
Φ (dense/medium dense)	40	35	30

As an example, the backbone curves of the springs under dense sand conditions are obtained as follows:

- The friction angle of soil is taken as 40^0 for dense sand.
- The density of dense sand is 20 kN/m^3. (Bowles, 1996)
- The embedment is taken by 6 meters.
- By the use of the formulae mentioned in the previous section, the necessary parameters to calculate the bearing capacity under both elastic and inelastic regions are found as follows:

  Equation (2) states that;

$q_0 = C_r q_{ult}$ where q_0 and C_r stand for the load at the yield point and a constitutive parameter, respectively. After passing the yield point, the inelastic range starts.

The constitutive parameter C_r is taken as 0.36 from Table 1. The ultimate bearing capacity is calculated by the use of the equation (7):

In equation (7), the cohesion parameter, c is equal to zero. Since sand is a cohesionless material, the first term in the equation equals zero. The angle of friction, density of dense sand and embedment depth are given in the previous section. In order to calculate the ultimate bearing capacity, the flow number, N, has to be calculated. The value of flow number is calculated as follows:

$$N = \frac{1 + sin40}{1 - sin40} \approx 4.60$$

After calculating the flow number, transverse and axial loads which are resisted by the pier are calculated. These values are 8654 kN abd 47169 kN, respectively. The values obtained here are used in the formula mentioned as follows:

$$q_{ult} = 20 \times 6 \times \frac{1 + sin40}{1 - sin40} e^{\pi tan40} \times \left(1 + \frac{10}{14} \times sin40\right) \times \left[1 + (2 \times tan\emptyset \times (1 - sin\emptyset)^2) \times \frac{6}{10}\right] \times \left[1 - \frac{tan^{-1}\frac{8654}{47169}}{90}\right]^2 + 0.5 \times 20 \times 10 \times 1.5\left(N_q - 1\right)\tan(40) \times \left(1 - 0.4 \times \frac{10}{14}\right) \times 1 \times \left[1 - \frac{tan^{-1}\frac{8654}{47169}}{\emptyset}\right]^2 \approx 13035.2\ kN/m^2$$

The value found above as the ultimate bearing pressure for the foundation is multiplied by the area of the foundation and divided into 25 since the soil is

modelled by the use of 25 vertical springs and the force-deformation relationship of these springs are obtained.

$$F_{spring,vertical} = q_{ult} \times \frac{10 \times 14}{25} \approx 72997kN$$

$$q_0 = 0.36 \times 72997 \approx 26279\ kN$$

Up until the loading values reach q_0, $Q_{vertical}$ material behaves elastically. The elastic region of the backbone curve is determined by equation (1):

$$q = k_{in} z$$

At this stage, the stiffness value in the elastic range has to be computed in order to draw the elastic portion of the backbone curve. Gazetas' equation (1991) is given as follows in order to determine the vertical stiffness of the mechanistic springs:

$$K_z = \frac{GL}{1-\nu}\left[0.73 + 1.54\left(\frac{B}{L}\right)^{0.75}\right]$$

The shear modulus value of the dense sand is used as 224,000 kPa from table 4.2.

After the determination of shear modulus, the foundation stiffness of vertical springs is calculated as follows:

$$K_z = \frac{224 \times 10^3 \times 14}{1-0.35}\left[0.73 + 1.54\left(\frac{10}{14}\right)^{0.75}\right] \approx 9294.8\ kN/mm$$

$$z_0 = \frac{q_0}{K_z} \approx 146.7\ mm$$

After determining the elastic range of the backbone curve, the necessary steps are followed to draw the inelastic region of the backbone curve. Since the

ultimate bearing capacity is calculated in the previous step by the use of equation (7), it is not re-calculated again.

There is only one missing parameter in equation (6) which is z_{50}. It stands for the displacement at which 50% of the ultimate load is mobilized. Since the ultimate load, the load at the yield point, the constitutive parameters, c and n, are determined, z_{50} is calculated by rearranging the terms of equation (6) as follows:

$$q_{50} = q_{ult} - (q_{ult} - q_0)\left[\frac{cz_{50}}{cz_{50} + |z_{50} - z_0|}\right]^n$$

$$q_{50} = \frac{q_{ult}}{2} \approx 36499kN$$

From the equation above, by the use of Goal Seek feature of Excel, z_{50} is calculated as 255 mm.

Since the parameters to draw the elastic and inelastic regions of the backbone curve are determined, the following load vs displacement curve of $Q_{vertical}$ material is obtained as follows:

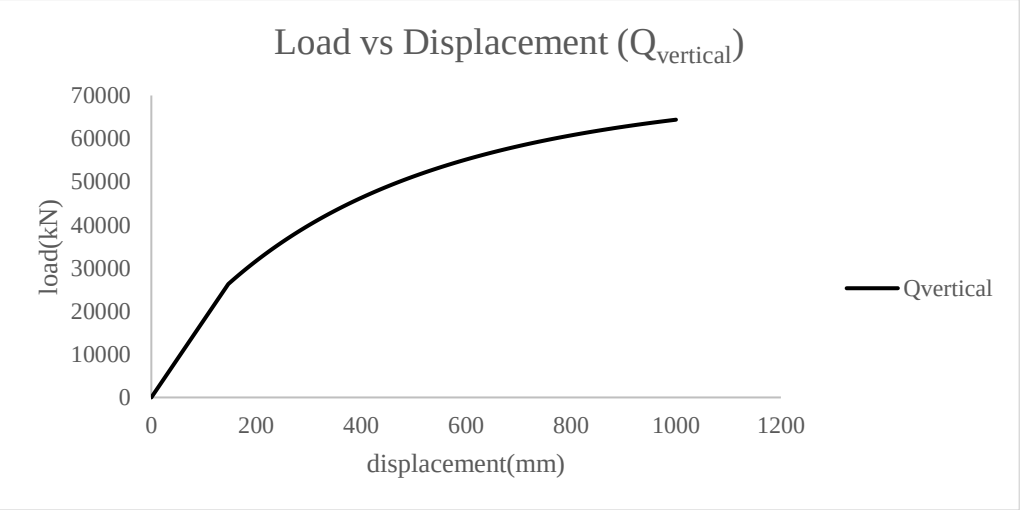

Figure 14. Load vs Displacement Curve of Qvertical Element

After determining the necessary parameters for the springs which work vertically, the springs which work for horizontal passive load-displacement behavior are explained below:
In the elastic range, equation (24) holds true which is:

$$p = k_{in}u \tag{24}$$

This time, equation (1) is used to calculate lateral displacement. The load at the yield point, p_0 is calculated by the use of equation (24).

$$p_{ult} = 0.5\gamma D_f^2 K_p \tag{25}$$

$$p_{ult} = 0.5 \times 20 \times 6^2 \times tan^2\left(45 + \frac{40}{2}\right) \approx 1655.6\ kN/m$$

These springs work in lateral direction and model the passive pressure of the soil. Two P_{slide} springs are used in this model and they are locaed on both sides of the foundation. The force of a single spring is calculated by multiplying the ultimate passive pressure by the length of the footing.

$$F_{spring,slide} \approx 23178.5\ kN$$

$$p_0 = C_r \times P_{ult} = 0.33 \times 23178.5 \approx 7648.9\ kN$$

At this point, the elastic stiffness parameter of P_{slide} material has to be found by the use of equation (5) in order to draw the elastic portion of the backbone curve.

$$K_x = \frac{224 \times 14 \times 10^3}{2 - 0.35} \times \left[2 + 2.5\left(\frac{10}{14}\right)^{0.85}\right]$$

$$K_x = 7370.8\ kN/mm$$

$$u_0 = \frac{p_0}{k_{in}} = \frac{7648.9}{7370.8} \approx 1.038mm$$

In order to determine the inelastic range, the displacement at which 50% of the ultimate load is mobilized (z_{50}), has to be found. By the use of equation (6) and Goal Seek tab of Excel, z_{50} is calculated as 0.043 mm.

By using the equations (1) and (6), the backbone curve is obtained and the following load-displacement graph of P_{slide} material is shown as follows:

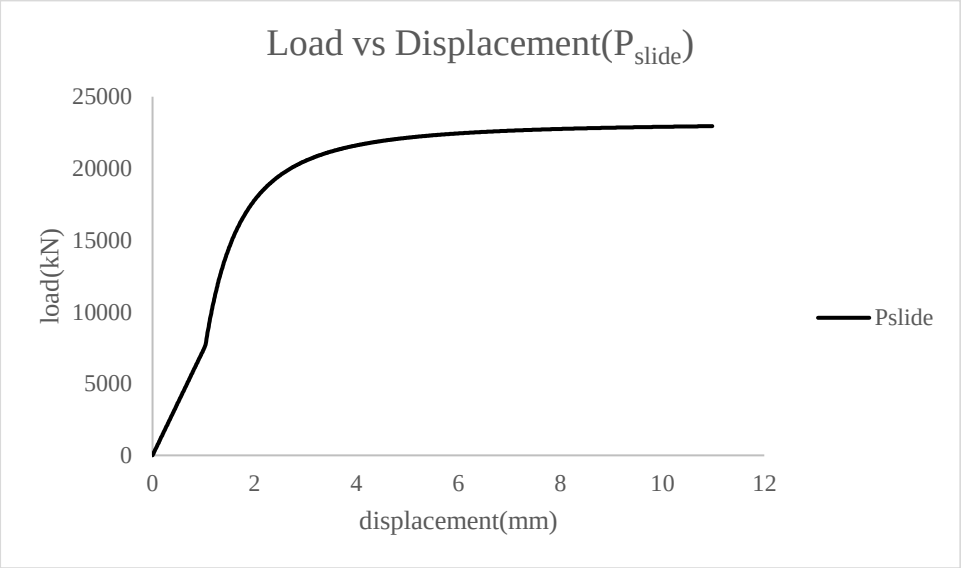

Figure 15. Load vs Displacement Curve of Pslide Element

After determining the parameters for both $Q_{vertical}$ and P_{slide}, the necessary parameters are determined for the springs which work for horizontal shear-sliding behavior as follows:

In the elastic range, equation (26) holds true which is:

$$t = k_{in} u_0 \quad (26)$$

In order to find the yield point, the ultimate load has to be calculated as shown previously by the use of equation (20):

$$t_{ult} = 47169kN \times tan\left(\frac{40}{2}\right) \approx 17168\ kN$$

$$t_0 = C_r \times t_{ult} = 0.48 \times 17168 \approx 8240.7\ kN$$

$$K_y = \frac{224 \times 14 \times 10^3}{2 - 0.35}\left[2 + 2.5\left(\frac{10}{14}\right)^{0.85}\right] + \frac{224 \times 14 \times 10^3}{0.75 - 0.35}\left[0.1 \times \left(1 - \frac{10}{14}\right)\right]$$

$$K_y = 7594.8\ kN/mm$$

$$u_0 = \frac{8240.7}{7594.8} \approx 1.085mm$$

In order to determine the inelastic range, the displacement at which 50% of the ultimate load is mobilized (z_{50}), has to be found. By the use of equation (6) and Goal Seek tab of Excel, z_{50} is calculated as 1.1 mm approximately.

By using the equations (1) and (6), the backbone curve is obtained and the following load-displacement graph of TzSimple1 material is shown as follows:

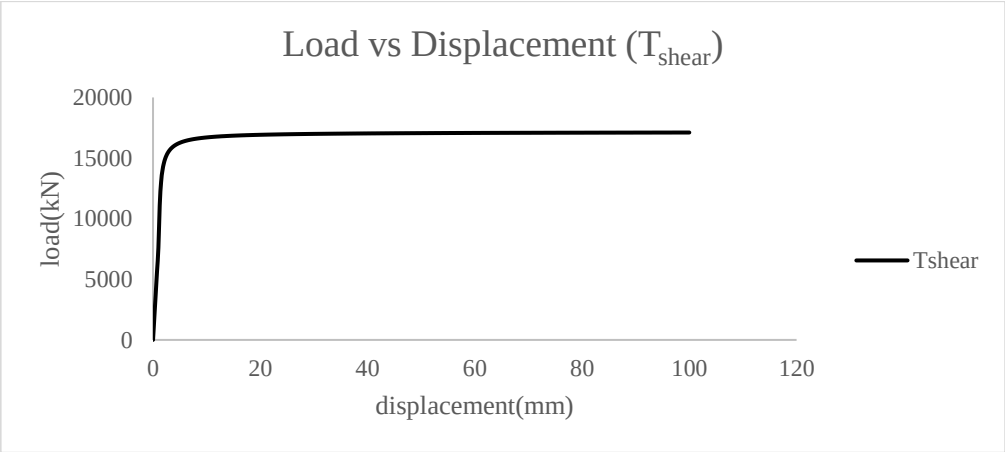

Figure 16. Load vs Displacement Curve of Tshear Element

CHAPTER 5

MODELLING OF THE BRIDGES

In this chapter, the modelling phases of the foundation, aubtment and the piers are introduced. Eskişehir Köseköy Bridge is the benchmark bridge according to the statistical analyses conducted in this thesis. In order to observe the effects of rocking,the foundations of the piers are changed.

First, the modelling phase of the foundation is explained. After this explanation, the simplistic design of the abutment is explained. In the last step, the design of multiple column pier bent is explained to the reader.

5.1. Modeling of the Foundation

The original bridge has identical foundations with the dimensions of 16 meters to 20 meters. But since the effect of rocking is studied in this thesis, the footings are changed according to the formulae of Meyerhof, and Brinch Hansen (Salgado,2003).

For dense, medium dense and loose sand types, three different foundation dimensions are calculated.

In order to design the foundation, the capacity design is made. In this step, the ultimate bearing capacity of the foundation has to be calculated. This calculation is done by the formulae of Meyerhof and Brinch Hansen. (Salgado,2003)

Before heading into the chart which gives the value of the ultimate pressure of the foundation, necessary parameters and the formulae are explained as follows:

Bearing capacity of the footings in sand can be calculated by the formulae of Meyerhof and Brinch Hansen. In this study, a hybrid formula is used which contains multipliers from both of the formulae. Since Meyerhof's formula is upgraded by the experiments conducted in the field, new parameters are taken from Brinch Hansen's formula.

The friction angle values for dense, medium dense and loose sand conditions are used as 40^0,35^0 and 30^0, respectively (FHWA,1986).
The flow number, N, is calculated as follows:

$$N = \frac{1+sin\emptyset}{1-sin\emptyset} \quad (27)$$

Bearing capacity factor, N_q, is obtained by the use of the flow number as follows:

$$N_q = \frac{1+sin\emptyset}{1-sin\emptyset} e^{\pi tan\emptyset} \quad (28)$$

Since these calculations are done for dense sand, friction angle, ϕ, is taken as 40^0. Hence, N equals 4.6.

After the calculation of N, the shape, depth and inclinations factors are taken into consideration. Shape and depth factors, s_q and d_q respectively, are calculated by the formula of Brinch Hansen whereas the inclination factor is calculated by the formula of Meyerhof.

$$s_q = 1 + \frac{B}{L} sin\emptyset \quad (29)$$

In the shape factors, the breadth value is not equal to the actual value of 10 meters under dense sand conditions. In capacity design, the dimensions "B" and "L" are determined by the direction of loading. In transverse loading conditions, the dimension "B" is equal to 1.27 meters and the longitudinal direction is equal to 10 meters.

If D/B, which is the ratio of the depth of the foundation to the breadth of the footing, is smaller than 1, the following formula governs for the depth factor:

$$d_q = 1 + 2tan\emptyset(1 - sin\emptyset)^2 \frac{D}{B} \quad (30)$$

If D/B is larger than 1, the following formula governs:

$$d_q = 1 + 2tan\emptyset(1 - sin\emptyset)^2 tan^{-1} \frac{D}{B} \quad (31)$$

The inclination factor, i_q, is given as follows:

$$i_q = \left[1 - \frac{arctan\left(\frac{Q_{tr}}{Q_{axisl}}\right)}{90}\right]^2 \quad (32)$$

The inclination factor consists of two parameters which are the transverse loading and the axial loading. Transverse loading is the summation of two components. First component is obtained by dividing the plastic moment capacity into the total height of the pier, cap beam and pedestal. Second component is the footing inertial force which is calculated from the mutliplication of the weight of the footing by the peak ground acceleration which is equal to 0.35.

Table 5.1. Ultimate Bearing Capacity of The Footing Under Dense Sand Conditions

CAPACITY DESIGN OF THE FOUNDATION (DENSE SAND)	
Density (kN/m^3)	20
Depth of the Foundation (D_f,m)	6
Angle of Friction (ϕ)	40
N_q	64.2
N	4.6
B(m)	1.27
L(m)	10
F_{qs}	1.081
F_{qd}	1.292
F_{qi}	0.694
N_γ	79.5
$F_{\gamma s}$	0.95
$F_{\gamma d}$	1
$F_{\gamma i}$	0.39
q_{ult} (kPa)	7842

Same procedure is followed in the calculation phases of the capacity design of the foundations under medium dense and loose sand conditions. The results are tabulated as follows:

Table 5.2. Ultimate Bearing Capacity of The Footing Under Medium Dense Sand Conditions

CAPACITY DESIGN OF THE FOUNDATION (MEDIUM DENSE SAND)	
Density (kN/m^3)	18
Depth of the Foundation (D_f,m)	6
Angle of Friction (φ)	35
N_q	33.3
N	3.69
B(m)	1.54
L(m)	11
F_{qs}	1.081
F_{qd}	1.336
F_{qi}	0.692
N_γ	33.9
$F_{\gamma s}$	0.94
$F_{\gamma d}$	1
$F_{\gamma i}$	0.32
q_{ult} (kPa)	3736

Table 5.3. Ultimate Bearing Capacity of The Footing Under Loose Sand Conditions

CAPACITY DESIGN OF THE FOUNDATION (LOOSE SAND)	
Density (kN/m^3)	16
Depth of the Foundation (D_f,m)	6
Angle of Friction (φ)	30
N_q	18.4
N	3
B(m)	2.61
L(m)	11
F_{qs}	1.119
F_{qd}	1.335
F_{qi}	0.678
N_γ	15.07
$F_{\gamma s}$	0.905
$F_{\gamma d}$	1
$F_{\gamma i}$	0.222
q_{ult} (kPa)	1852

5.2. Modeling of the Abutment

The abutment of the bridge is modelled with a simplistic design philosophy. First, both the abutment and the wingwalls are modelled with their components. The abutment modelled in this study is represented below. That model consists of horizontal and vertical abutment elements. Furthermore, the wingwalls are modelled by the use of the same method with horizontal and vertical wingwall elements. Both the abutment horizontal elements and the horizontal wingwall elements have sufficient inertia but they are massless. The vertical elements of both the wingwall the abutment have mass and inertia. The following figures show the full abutment modelling in longitudinal and transverse directions. For both directions, the abutment-backfill relationships are modelled as shown:

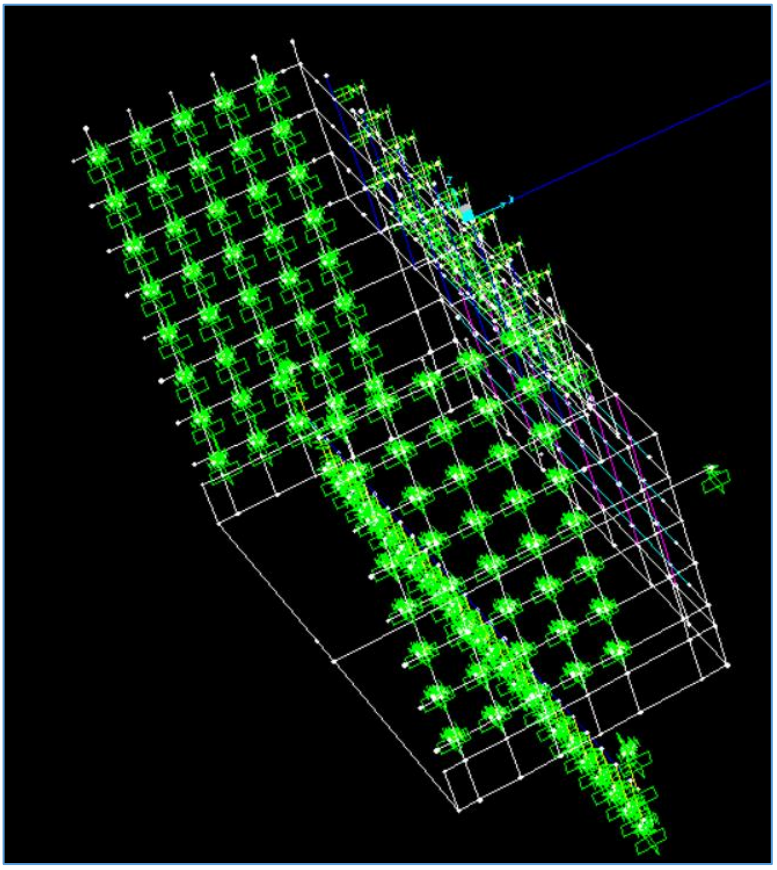

Figure 17. Full Scaled Model of an Abutment in Transverse Direction

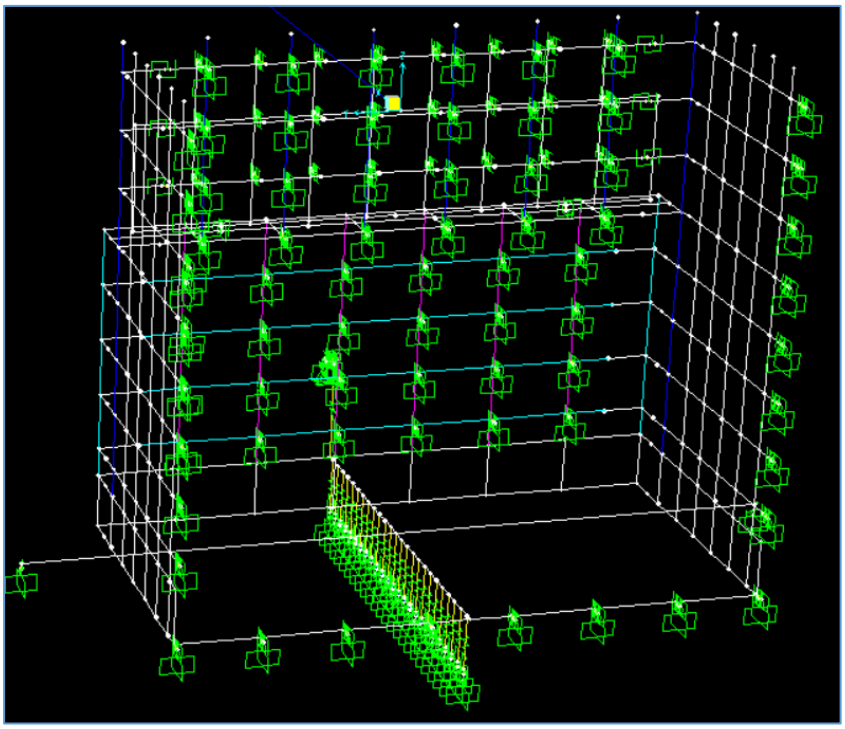

Figure 18. Full Scaled Model of an Abutment in Longitudinal Direction

The members located on the wingwalls of the model in transverse and longitudinal directions are created by the model of Coll and Rollins (2006). Since the model of Coll and Rollins is developed on a pile cap with dimensions of 1.12 m to 5.18 meters, the model is adapted to the abutment considered in the thesis. The cross sectional area considered in Coll and Rollins' model is 5.8 m^2. The height of the abutment considered in the thesis is 10.4 meters and the width of the abutment is 12 meters. Hence, the cross-sectional area of the abutment is 21.5 times larger than the sample of Coll and Rollins' model. It is noteworthy that a single maximum stiffness value for coarse gravel is given by Coll and Rollins (2006) which equals 259 kN/mm but this value cannot be used for the abutment considered in the thesis. Hence, the maximum stiffness of the backfill equals 5,572,966 kN/m. This value is the resultant of the stifness value of nine layers in total and every single layer is divided into eight equal pieces with dimensions of 1.5 meters in width and 1.05 meters in height. The passive earth pressure coefficient is taken as 14 and this value is verified by Lemitzer's tests

(2009) on abutments. R_f which is the failure ratio is taken as 0.85. The density of the backfill considered in this study is taken as 20 kN/m^3.

The force applied on a tributary area is computed by the following formula:

$$F_T = \frac{1}{2} K_p \gamma z A_T \quad (33)$$

Here, "A_T" represents the tributary area and z represents the depth.

The ultimate force measured on the abutment is calculated as follows:

$$F_{ult} = \frac{1}{2} K_p \gamma H^2 w \quad (34)$$

Here, "w" represents the width of the abutment and "H" represents the height of the wall.

The term "K_{spring}" represents the stiffness of the considered layer. It is calculated as follows:

$$K_{spring} = K_{max} \frac{F_T}{F_{ult}} \quad (35)$$

Cole and Rollins (2006) propose two terms which are Δ_s and Δ_p. These terms represent apparent soil movement and previous peak deflection, respectively. Apparent soil movement occurs at the end of the unloading stage and previous peak deflection occurs at the end of a loading cycle. In order to find the values of these two terms, an iterative process is followed. First, the term Δ_p is assigned. By the use of the formula given below, apparent soil movement is calculated:

$$\frac{\Delta_s}{\Delta_p} = \frac{(\Delta_p/H)}{0.0095+1.23(\Delta_p/H)} \quad (36)$$

After the calculation of apparent soil movement, the reloaded stiffness value is calculated as follows:

$$\frac{K_r}{K_{spring}} = 1 - \frac{(\Delta_s/H)}{0.0013+1.4(\Delta_s/H)} \quad (37)$$

This is the last stage for this algorithm since both maximum stiffness value for the considered layer and reloaded soil stiffness values are found.
These two stiffness values are used to calculate the alfa number which is used to locate the pivot point. Pivot point is used for the pushover link and it is going to be introduced to the reader.

$$\alpha = \frac{K_{r2} \cdot K_{r1}}{K_{r2} - K_{r1}} \cdot (\Delta_{s1} - \Delta_{s2}) \cdot \frac{1}{F_y} \quad (38)$$

After calculating the reloaded stiffness value, the force-deformation relationship can be assigned to the program SAP2000.

$$F_{layer1} = \frac{\Delta}{\frac{1}{K_{spring}} + R_f \frac{\Delta}{K_p \gamma z A_T}} \quad (39)$$

After introducing every single member in the calculation phase to obtain the force-deformation relationship in each layer, the soil and wall properties considered in this study are given as follows:

Table 5.4. Backfill Properties (Layer 1, z=0.525 m)

SOIL PROPERTIES	
Kmax(kN/m)	5572966
Rf	0.85
γ(kN/m^3)	20
Kp	14
F_{ult}(kN)	181709
F_t (kN)	232
K_{spring}(kN/m)	7101
Δ_s(m)	0.00147
Δ_p(m)	0.013
K_r(kN/m)	6679
A	24.52
B	-0.096
C	-0.00138
Δ_{int}(m)	0.0097

Table 5.5. The Wall Properties of The Backfill and The Backwall (Layer 1, z=0.525m)

WALL PROPERTIES	
z(m)	0.525
H(m)	10.4
w_tributary(m)	1.5
h_tributary(m)	1.05
A_tributary(m^2)	1.575
w_backwall(m)	12

The force-deformation relationship of the backfill for Layer 1 where the depth is 0.525 meters, is shown:

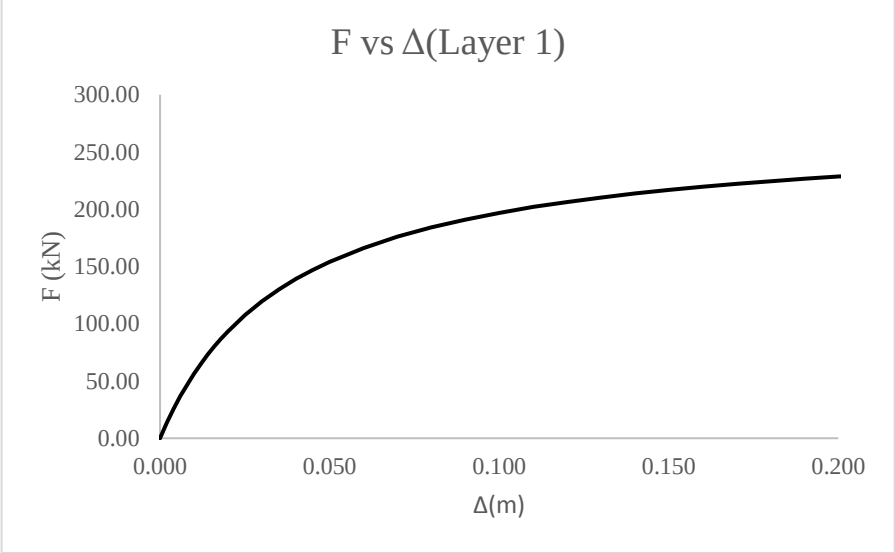

Figure 19. Force-Deformation Relationship of Layer 1

By following the same procedure explained in detail, the force deformation relationships of the other layers are obtained. And in order to reduce the run time, the simplistic method is applied. In this method, pushover analysis is conducted.

In the pushover analysis, the force values applied on each tributary area is calculated. The method of calculation is explained under "Modelling of the Abutment" section. The ultimate force applied on sliding spring (T_{shear}) is calculated. The summation of these two values is applied as a point load from the end of the deck. And under full load conditions, the force vs displacement of the joint at the left end of the deck is plotted. The plot is given as follows:

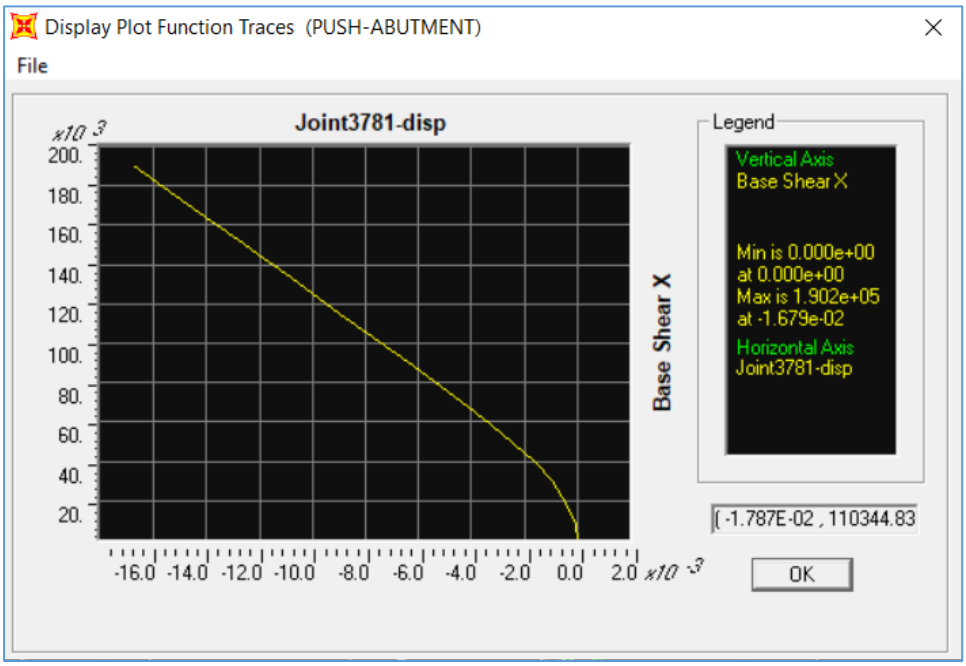

Figure 20. The Pushover Analysis Result

As it is given on the legend of the figure, the displacement can reach up to 1.7 centimeters when full load is applied.

Under cyclic loading conditions, the force-deformation curve shows that pivot point occurs. The figure below represents the force-deformation plot under cyclic loading conditions:

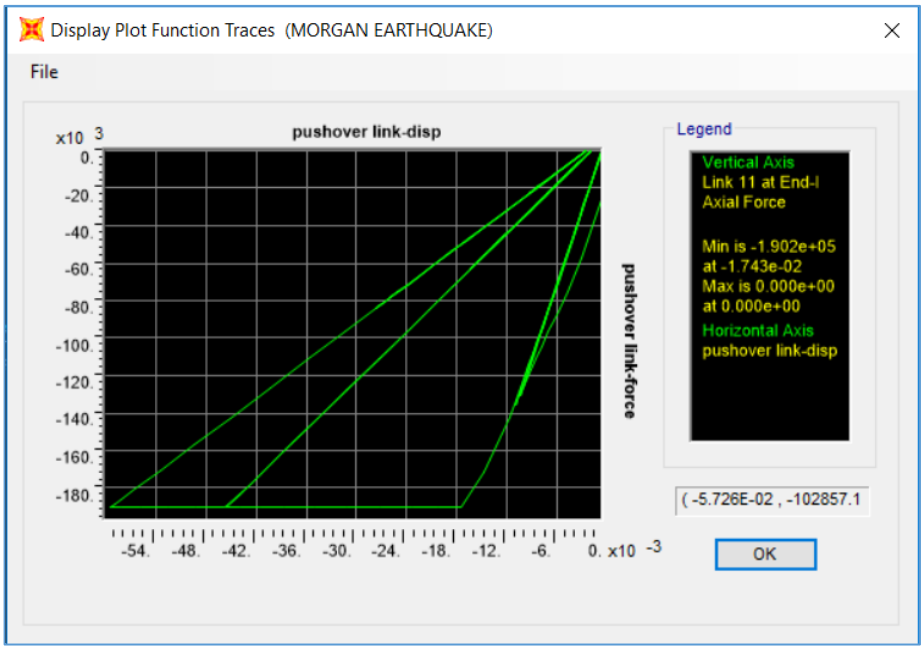

Figure 21. Force Deformation Relationship Under Cyclic Loading

The figure above represents the force deformation relationship under Morgan Earthquake. Since the displacement value is restricted by 1.7 centimeters the sudden cut on the x-axis is observed.

After the full abutment is shown, the simplistic design which reduces the run time significantly is shown:

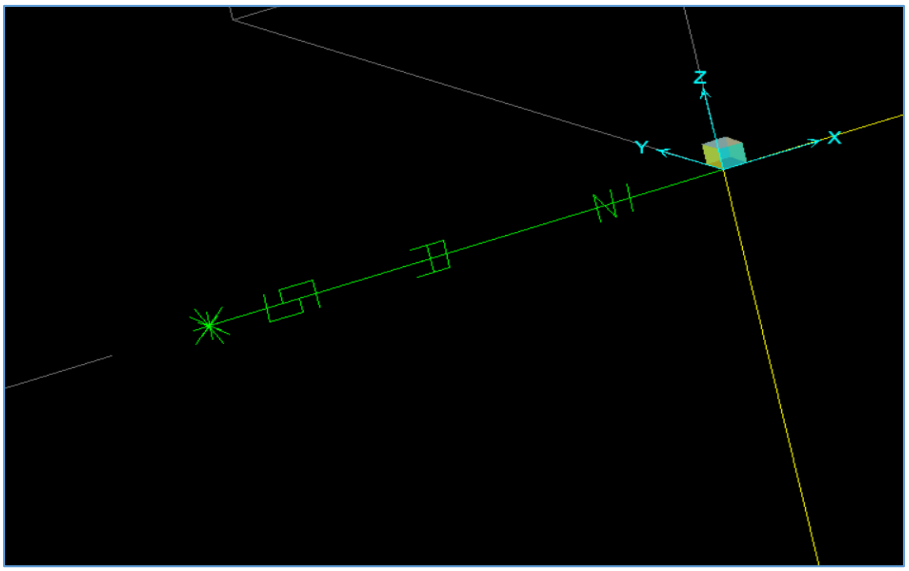

Figure 22. Simplistic Abutment Design

The connection mentioned in the last figure, consists of three major links which are the gap, damper and the pushover link. The gap and damper are defined as quite rigid in order to translate the force under seismic excitation to the pushover link. The force-deformation relationship is assigned to the link. The values of the force-deformation relationship are obtained from the pushover analysis.

5.3. Modeling of the Curved Surface Sliding Bearings

The curved surface sliding bearings (CSSB) are modeled by the use of plastic (Wen) model. They are located on the abutments.

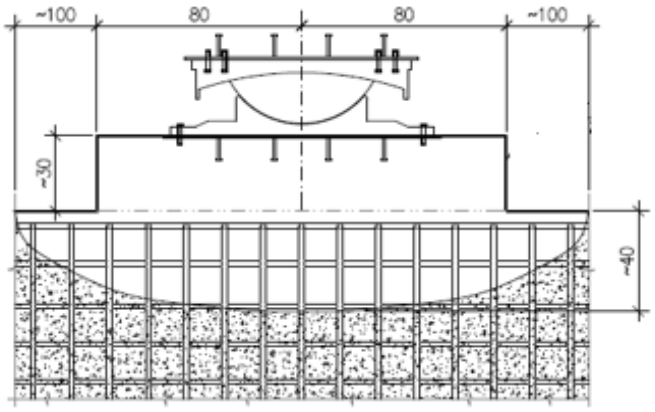

Figure 23. Curved Surface Sliding Bearings (CSSB)

The properties of the CSSB are given as follows:

$$k_{eff,linear} = \frac{\mu W}{D} + \frac{W}{R}$$

The load on the abutment is calculated as 7500 kN. Since there are two CSSB's located on the abutment, the weight is distributed equally and the term W equals 3750 kN. The friction coefficient is 0.12 and the design displacement, D, is 150 milimeters. The radius, R, is 2000 milimeters.

The linear effective stiffness equals 4875 kN/m.

Nonlinear stiffness value of the CSSB is calculated as follows:

$$k_{eff,nonlinear} = \frac{\mu W}{\Delta y}$$

Yield displacement of the CSSB is 2.5 milimeters. By the use of this value, nonlinear stiffness of the CSSB is calculated as 180000 kN/m.

The yield strength of the CSSB is calculated as follows:

$$F_y = \mu W + \frac{WD}{R}$$

The yield strength is calculated as 455 kN.

Post yield stiffness ratio is equal to 0.0104. These properties of the CSSB are assigned to sap2000.

5.4. Modeling of the Piers

Piers are taken from the original project but in order to observe the rotational behavior of the piers, Takeda links are used. Under cyclic loading, the rotational behavior of the pier can be obtained. These links are used in hammerhead piers and the cap beams in both longitudinal and transverse directions. Furthermore, they are used in multi-column pier bents in both directions.

The working mechanism of a Takeda link is explained as follows:
First, the ultimate and yield moment values of the hammerhead pier are calculated. After calculating the moment values, the corresponding curvature values are obtained. The chord rotation is taken into consideration. Since the area under moment-curvature diagram gives the moment-rotation diagram, the yield rotation and the ultimate rotation values are obtained.

By the use of these values, moment-rotation graph is obtained and these values are assigned to sap2000.

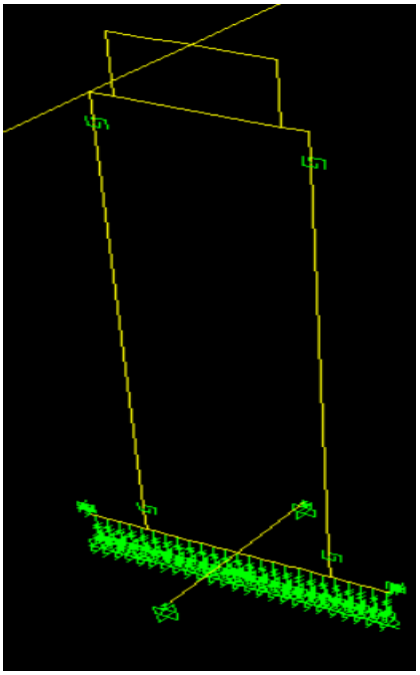

Figure 24. Takeda Link on Multi-Column Pier Bent

Figure 25. Takeda Link Located on the Cap Beam and Hammerhead Pier

The following three figures show the Takeda Link mechanism under 0.2 g, 0.35 g and 0.8 g peak ground acceleration in longitudinal loading.

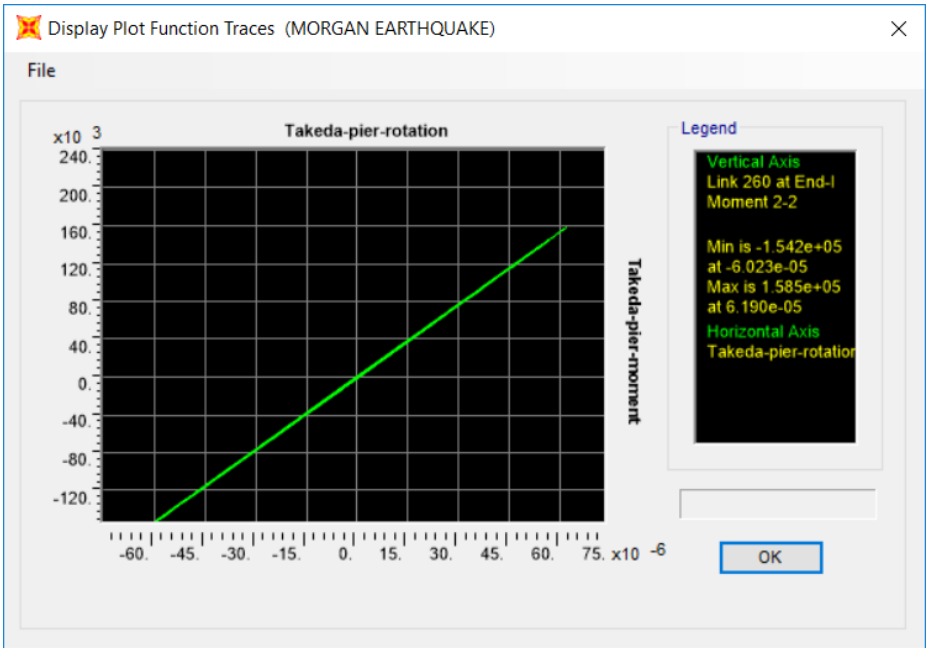

Figure 26. Takeda Link Moment-Rotation Results Under 0.2g (PGA)

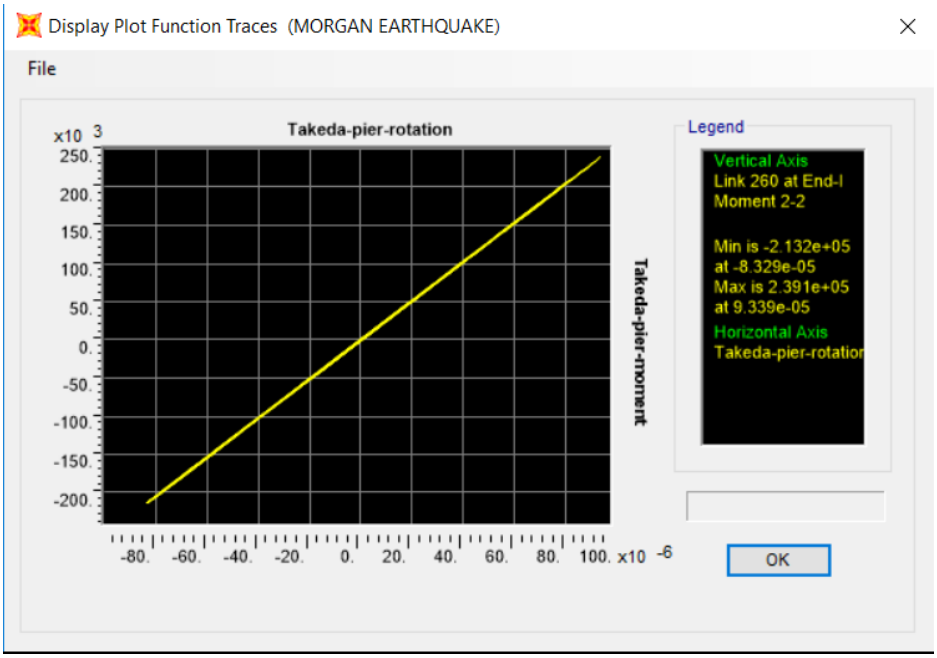

Figure 27. Takeda Link Moment-Rotation Results Under 0.35g (PGA)

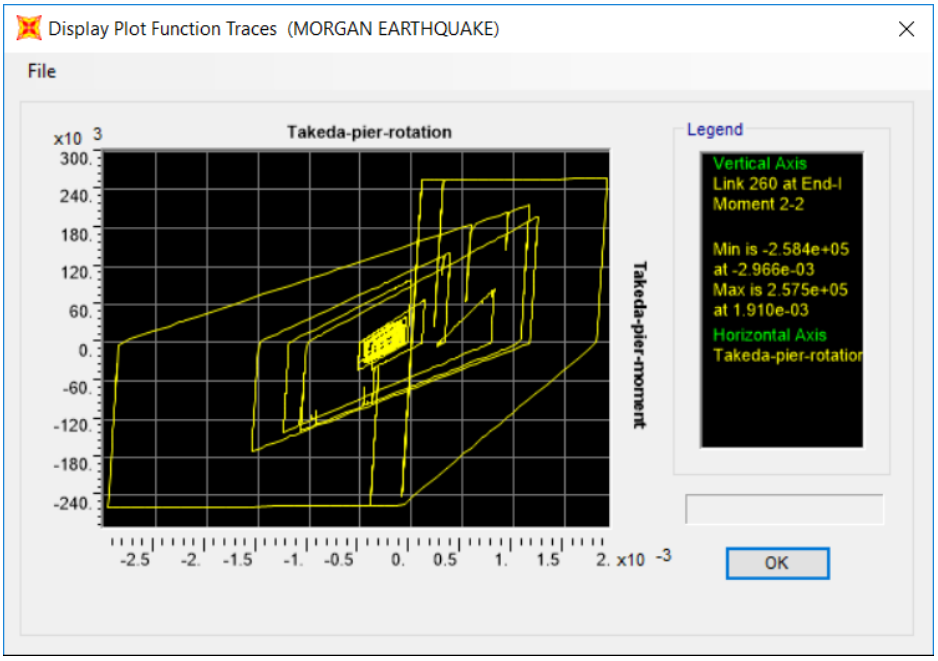

Figure 28. Takeda Link Moment-Rotation Results Under 0.8g (PGA)

CHAPTER 6

SELECTION OF DESIGN SPECTRA AND ASSOCIATED SETS OF GROUND MOTIONS

Design spectra are chosen from AASHTO (2012). The site classes are determined as “Site Class D” and “Site Class E”. Here, dense and medium dense sand are categorized under “Site Class D” and loose sand is categorized under “Site Class E”. Both of the spectra have the peak ground acceleration as 0.35 g. After the selection of the design spectra, seven ground motions are selected from the database of PEER Ground Motion Database. The properties of these ground motions are given as follows:

Table 6.1. Sets of Ground Motions for Soil Site Class D

Result ID	Year	Event	Magnitude	Station
1	1979	Imperial Valley	6.53	El Centro Array #13
2	1984	Morgan Hill	6.19	Capitola
3	1992	Landers	7.28	Desert Hot Springs
4	1992	Big Bear-01	6.46	Desert Hot Springs
5	1995	Kobe,Japan	6.9	Abeno
6	1999	Chi-Chi Taiwan	6.2	CHY039
7	1992	Joshua Tree	6.1	Indio-Jackson Road

Table 6.2. Sets of Ground Motions for Soil Site Class E

Result ID	Year	Event	Magnitude	Station
1	1987	Superstition Hills-02	6.54	Salton Sea Wildlife Refuge
2	1987	Superstiton Hills-02	6.54	Imperial Valley Wildlife Liquefaction Array
3	1999	Chi-Chi Taiwan-04	6.2	CHY047
4	1999	Chi-Chi Taiwan-04	6.2	CHY082
5	2010	El Mayor-Cucapah,Mexico	7.2	El Centro-Meloland Geotechnic
6	2010	El Mayor-Cucapah,Mexico	7.2	Westmorland Fire Station
7	2010	El Mayor-Cucapah,Mexico	7.2	El Centro Array #3

The AASHTO (2012) results and the acceleration response spectra of the selected sets of earthquakes for Soil Type D and Soil Type E are illustrated as follows:

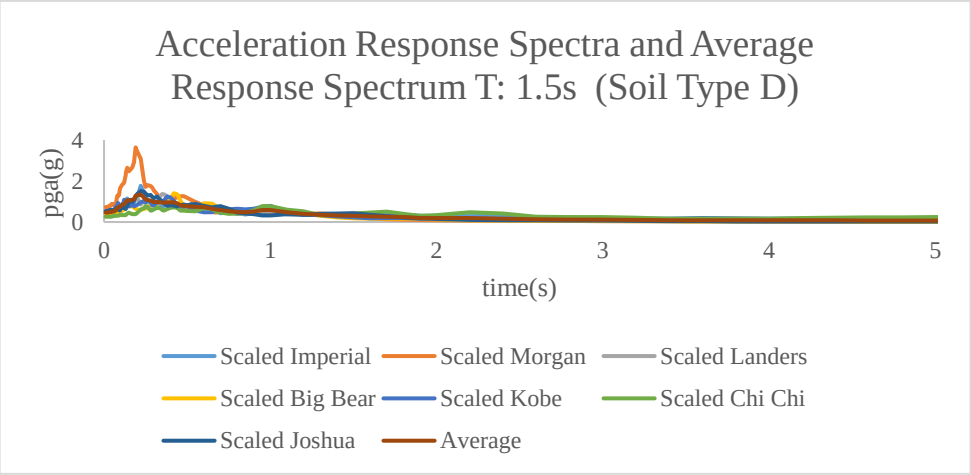

Figure 29. Acceleration Response Spectra and Average Response Spectrum of Soil Type D

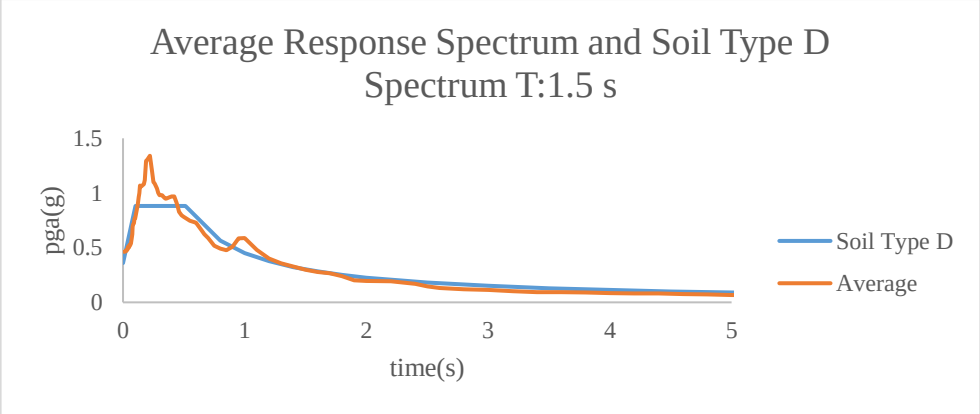

Figure 30. Average Response Spectrum and The Design Spectrum for Soil Type D

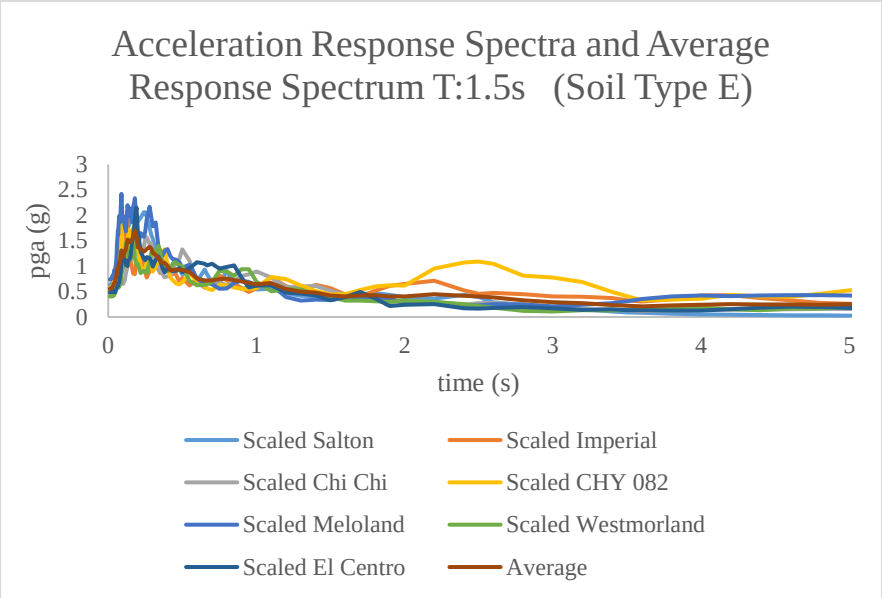

Figure 31. Acceleration Response Spectra and Average Response Spectrum of Soil Type E

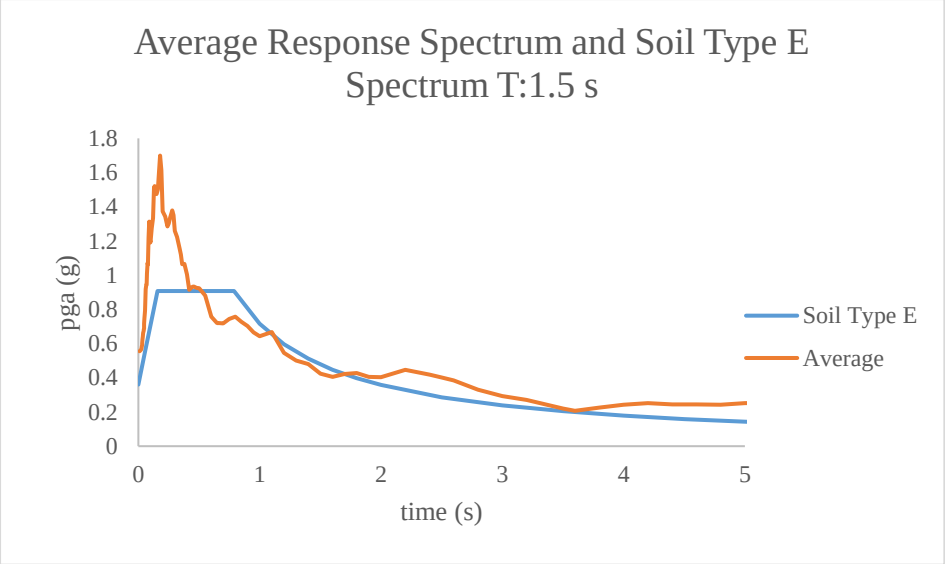

Figure 32. Average Response Spectrum and The Design Spectrum for Soil Type E

Table 6.3. Soil Spectra Parameters

	Site Class D	Site Class E
0.2 Sec, Spectral Acc, S_s	0.7094	0.7094
1 Sec, Spectral Acc, S1	0.2276	0.2276
Peak Ground Acc, PGA	0.2963	0.2963
Site Coefficient, F_a	1.2325	1.2812
Site Coefficient, F_v	1.9447	3.0895
Site Coefficient, F_{pga}	1.2073	1.2183
SDS=F_a x S_s	0.8743	0.9089
SD1=F_v x S1	0.4427	0.7033

CHAPTER 7

ANALYSES RESULTS

112 analyses are conducted in transverse direction and the results are tabulated as follows:

Under mediıum dense sand conditions, in transverse direction:

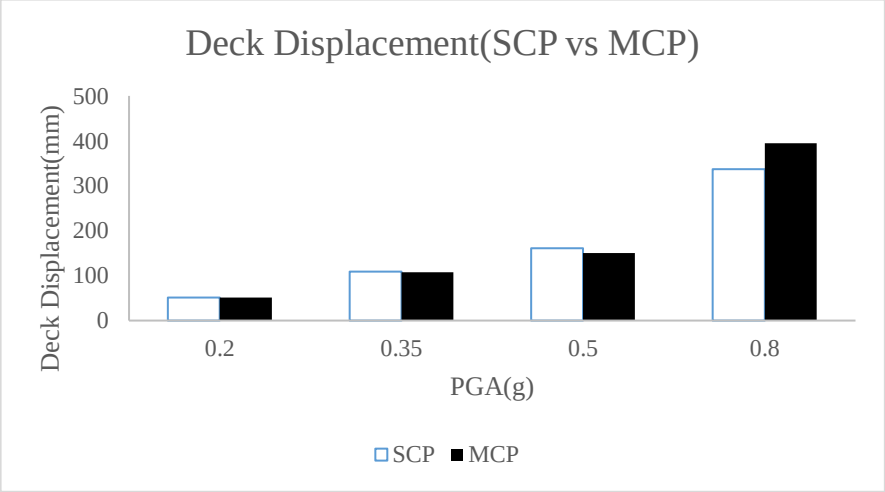

Figure 33. Deck Displacement (Single Column Pier versus Multiple Column Pier,Medium Dense Sand)

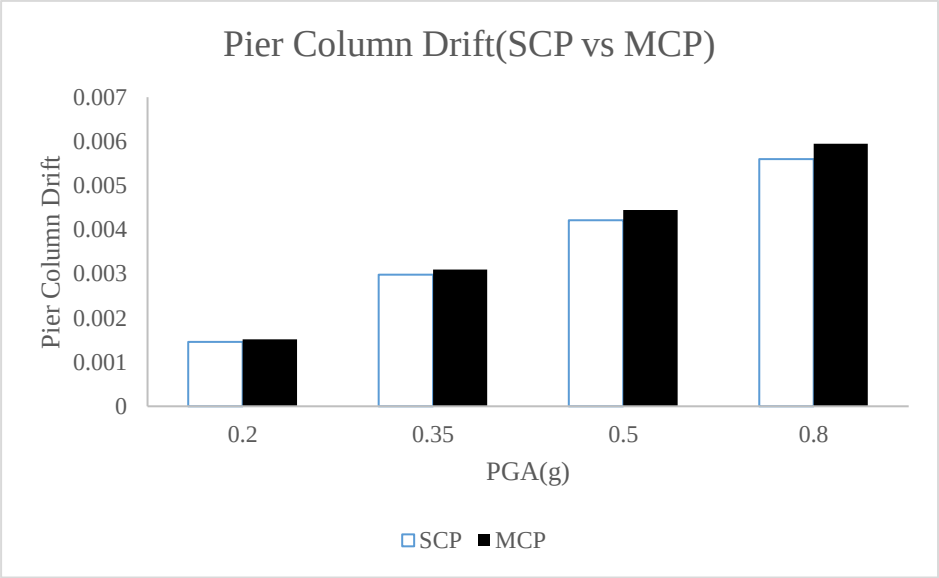

Figure 34. Pier Column Drift (Single Column Pier versus Multiple Column Pier,Medium Dense Sand)

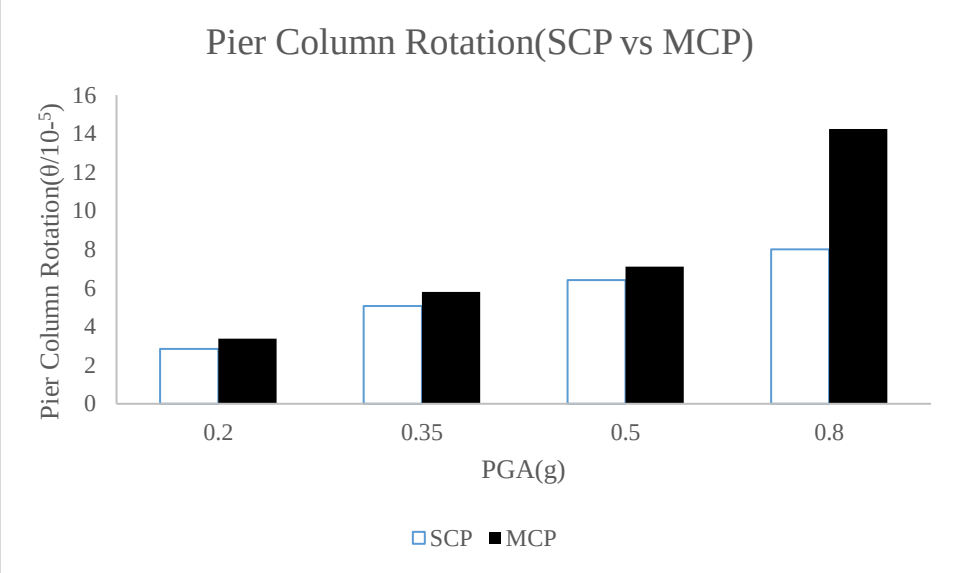

Figure 35. Pier Column Rotation (Single Column Pier versus Multiple Column Pier,Medium Dense Sand)

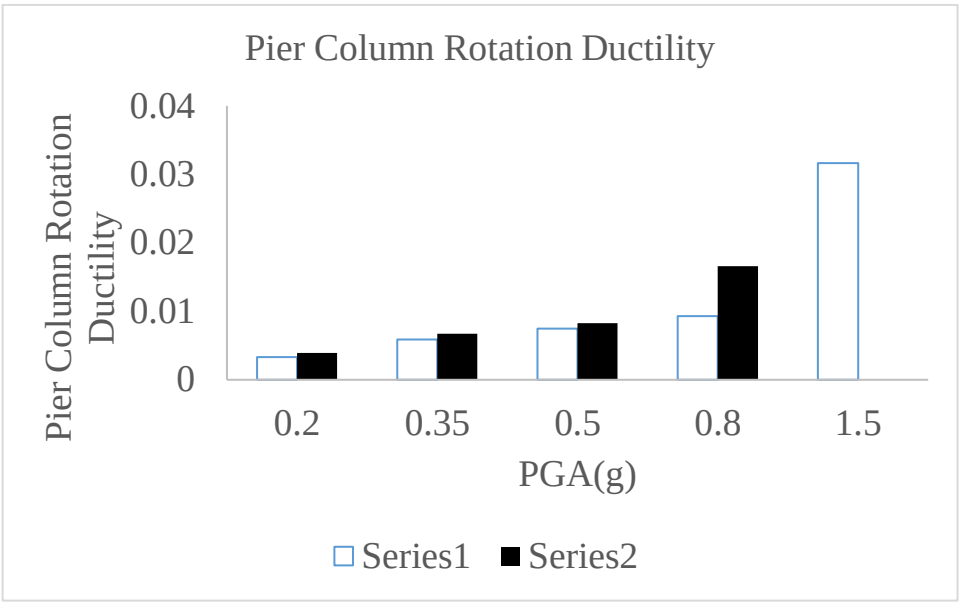

Figure 36. Pier Column Rotation Ductility (Single Column Pier versus Multiple Column Pier, Medium Dense Sand)

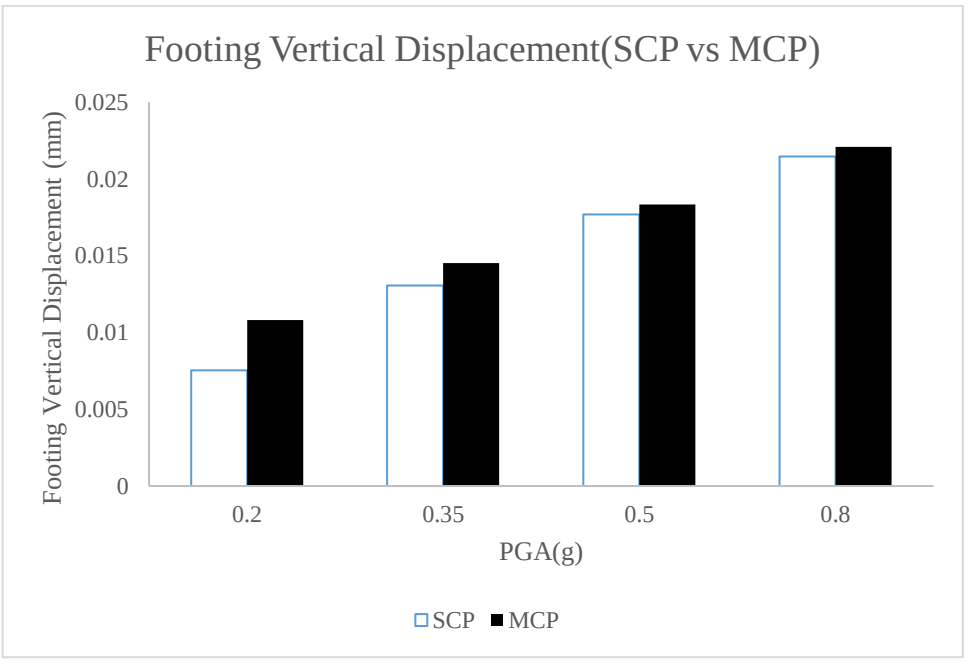

Figure 37. Footing Vertical Displacement (Single Column Pier versus Multiple Column Pier, Medium Dense Sand)

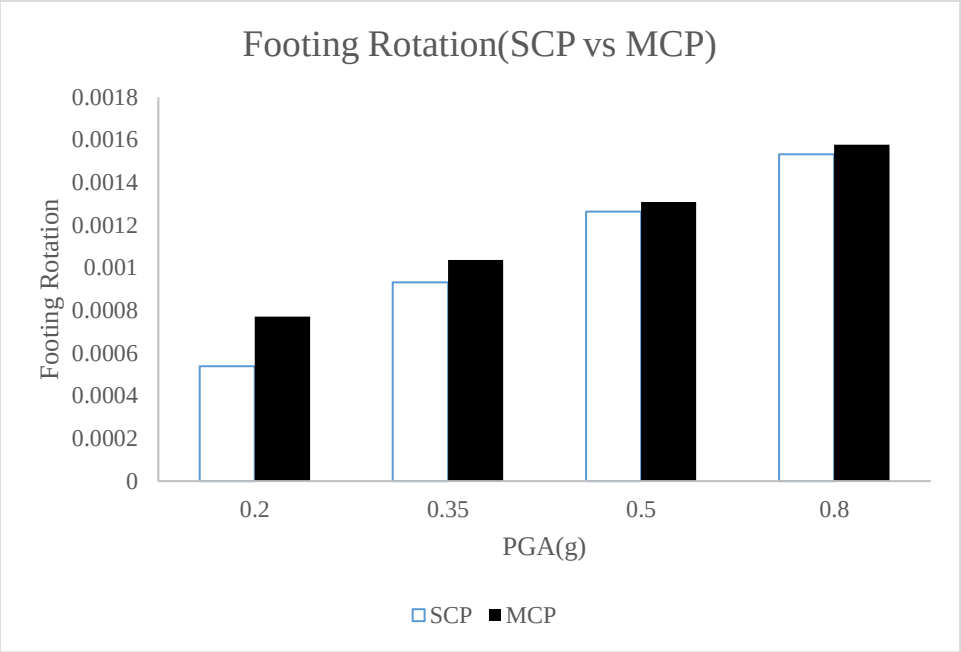

Figure 38. Footing Rotation (Single Column Pier versus Multiple Column Pier, Medium Dense Sand)

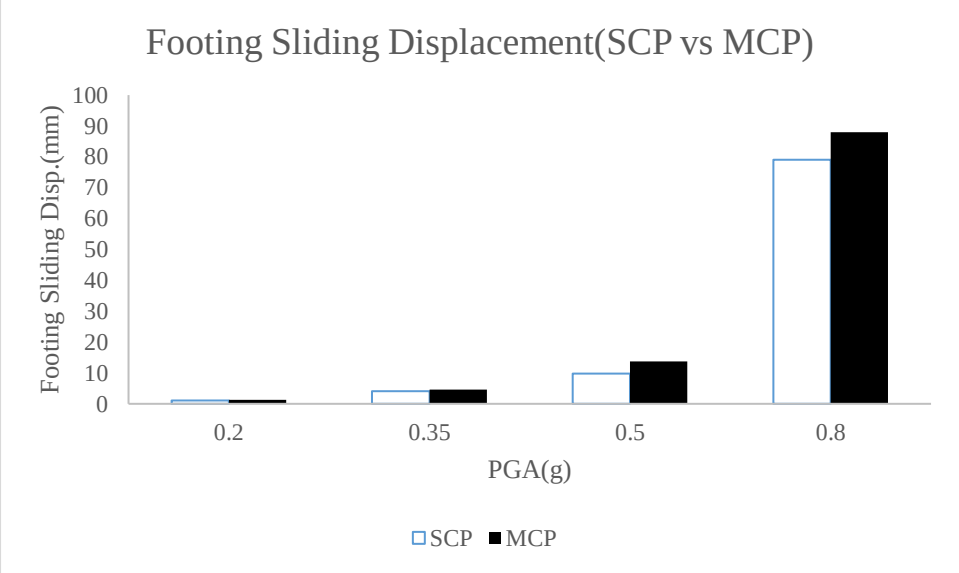

Figure 39. Footing Sliding Displacement (Single Column Pier versus Multiple Column Pier, Medium Dense Sand)

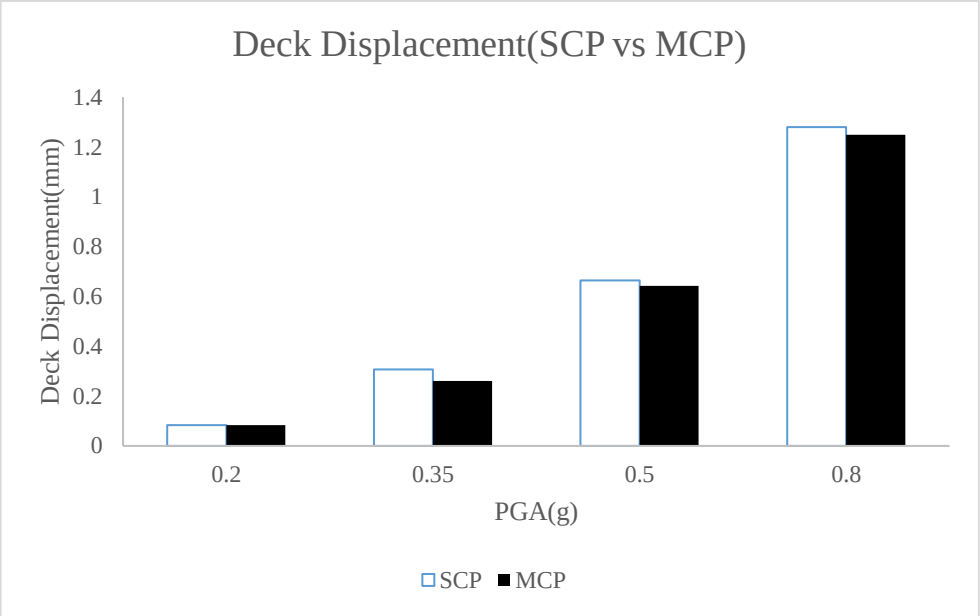

Figure 40. Deck Displacement (Single Column Pier versus Multiple Column Pier, Loose Sand)

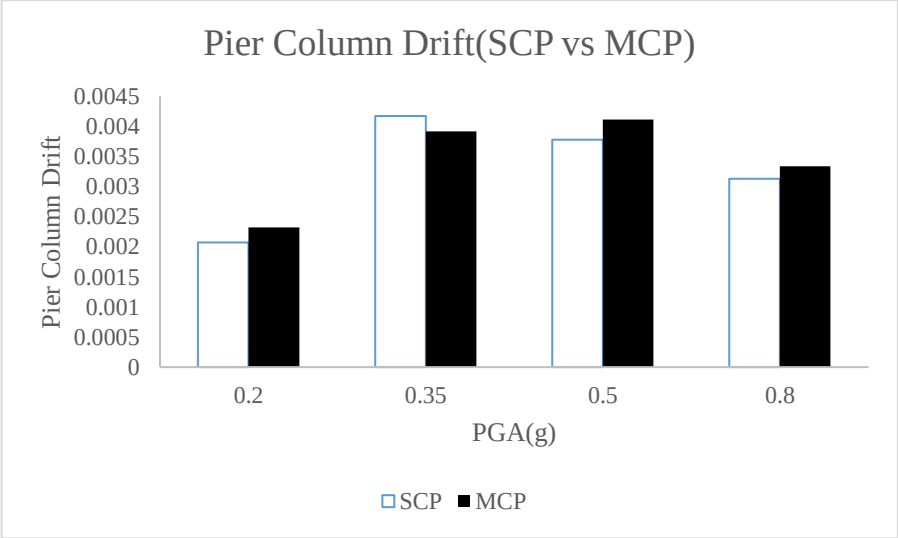

Figure 41. Pier Column Drift (Single Column Pier versus Multiple Column Pier, Loose Sand)

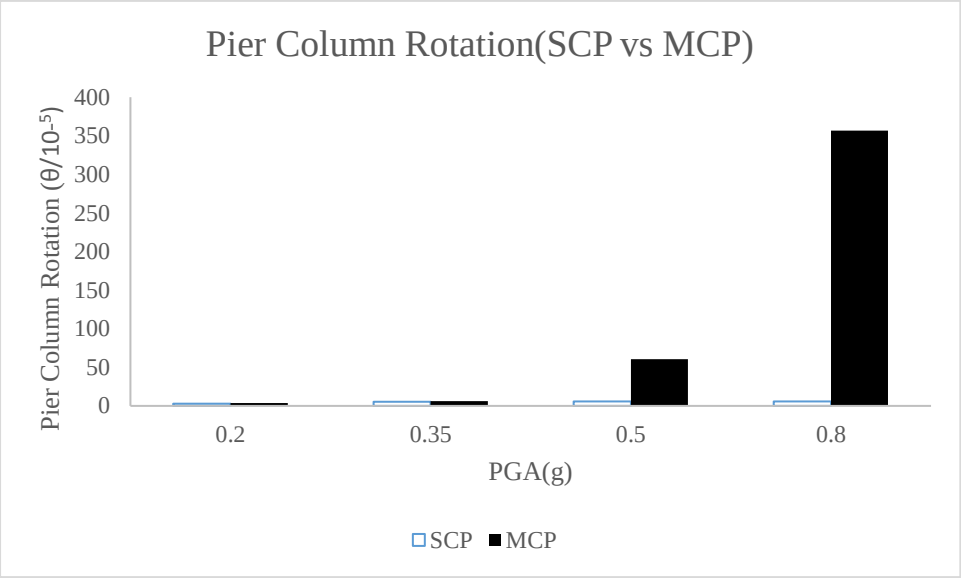

Figure 42. Pier Column Rotation (Single Column Pier versus Multiple Column Pier, Loose Sand)

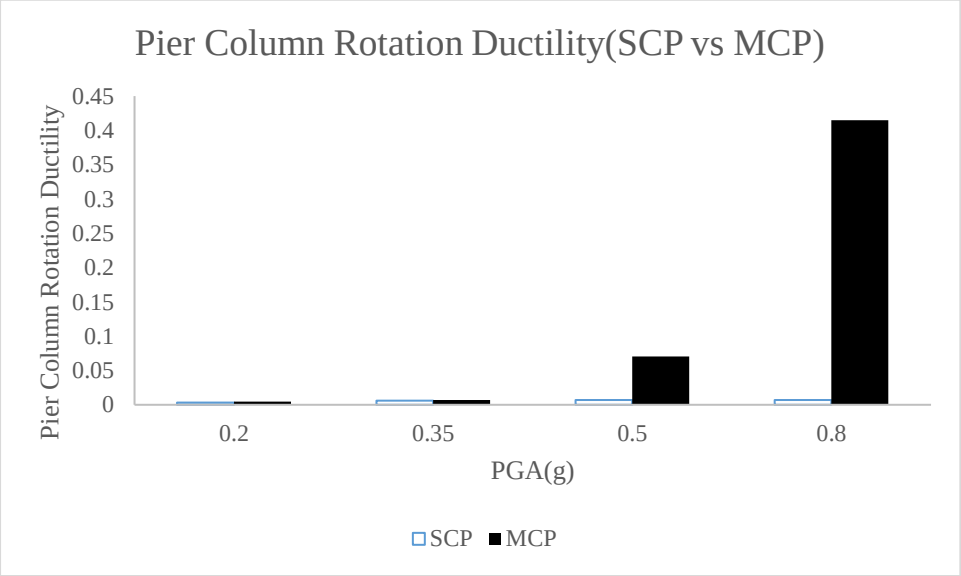

Figure 43. Pier Column Rotation Ductility (Single Column Pier versus Multiple Column Pier, Loose Sand)

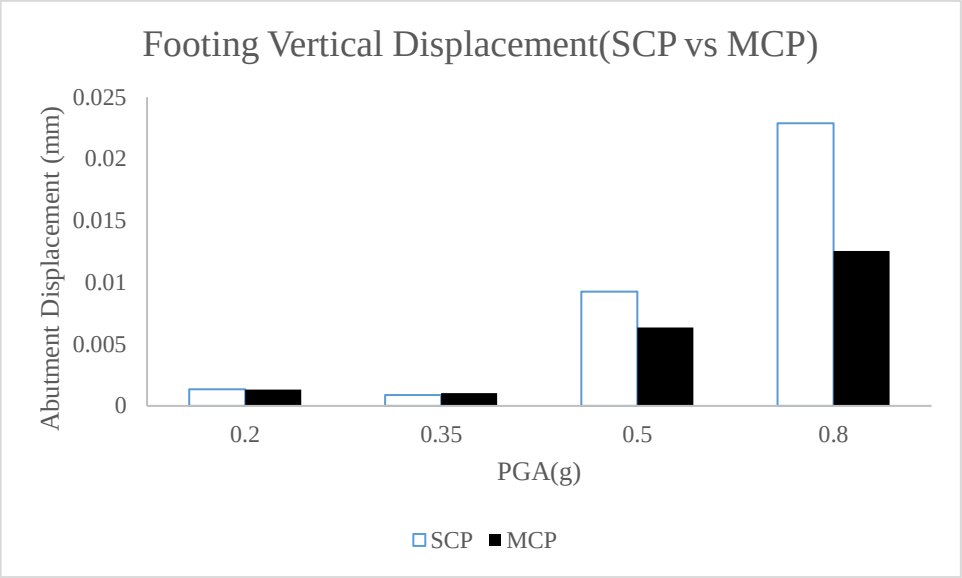

Figure 44. Footing Vertical Displacement (Single Column Pier versus Multiple Column Pier, Loose Sand)

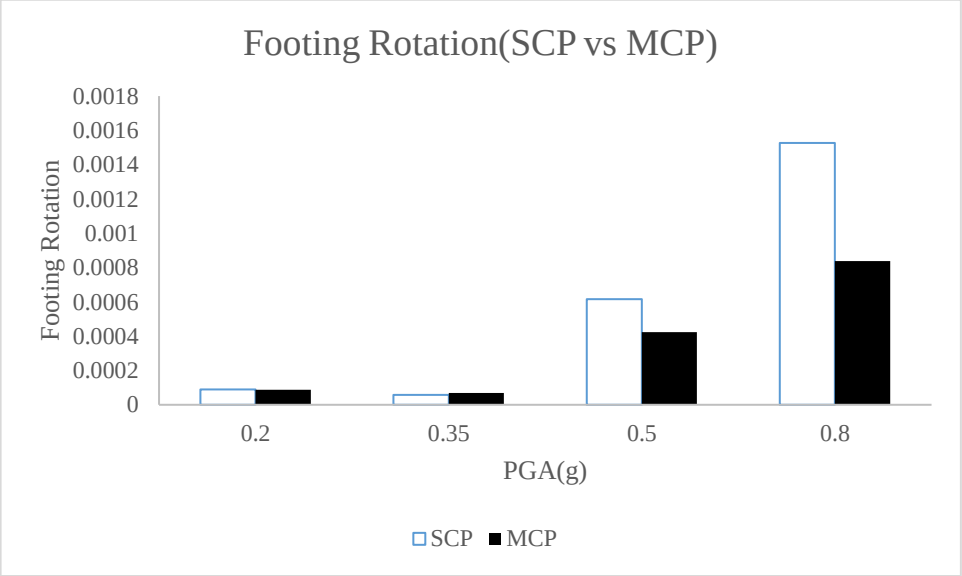

Figure 45. Footing Rotation (Single Column Pier versus Multiple Column Pier, Loose Sand

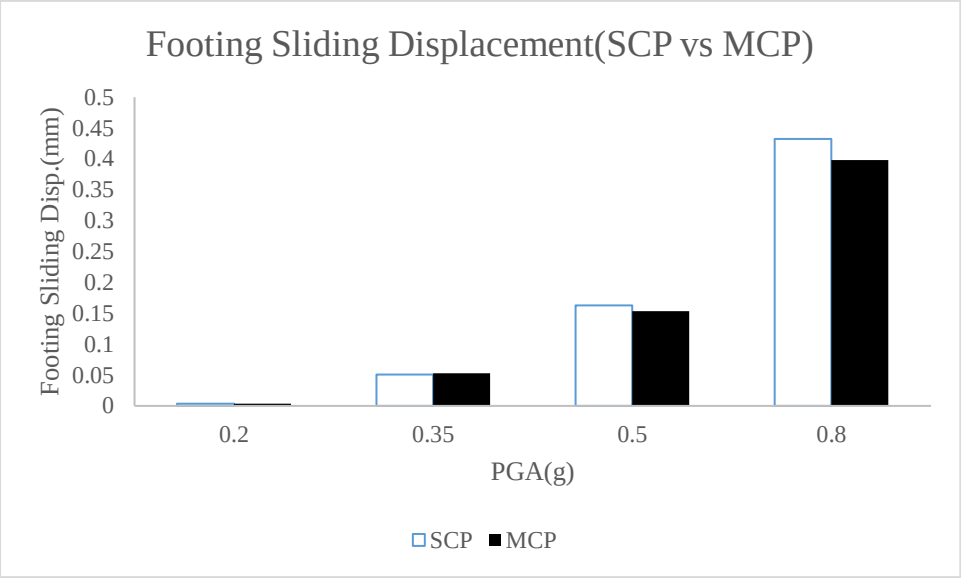

Figure 46. Footing Sliding Displacement (Single Column Pier versus Multiple Column Pier, Loose Sand)

According to Figure 33, deck displacement significantly increases under 0.8g peak ground acceleration. Under every peak ground acceleration given to the bridges, multi-column pier bent always shows more drift compared to hammerhead pier. In Figure 35, it is obvious that multiple column pier bent rotates more than single column pier. In Figure 36, the ductility level cannot be reached at any peak ground acceleration since under the the characteristic compressive strength of C25 concrete and yield strength of steel are input to the system as 32.48 MPa and 503 MPa because according to the article of Yücemen and Fırat (2014), the average values come as 32.48 MPa and 503 MPa, respectively. Furthermore, the bridge considered in this study is designed for 0.35g peak ground acceleration. Hence, the resistance of the bridges rises up to 0.5g. Moreover, in every analysis under 1.5g peak ground acceleration, soil yielded. Hence, the pier cannot yield because the soil yielded first. Figures 37 and 38 show that footing shows more displacement in the analyses conducted by single column pier. In Figure 39, footing shows large displacement when the peak ground acceleration reaches 0.8g.

CHAPTER 8

CONCLUSION

In this thesis, comparative seismic performance assessment of continuous slab on girder bridges with multi column pier bent and hammerhead pier for soft and stiff soil conditions is studied. Based on this study, the soil-structure interaction is taken into account in order to model the structure realistically. 112 analyses are conducted under medium and loose conditions of soil in transverse direction and conclusion is drawn as follows:

Despite the fact that the piers are designed for 0.35 g in real life, majority of the piers did not yield under seismic excitation. This might occur since the mean yield strength of steel is taken as 503 MPa and the characteristic compressive strength of C25 concrete, is taken as 32.48 MPa. These two parameters might increase the yield point.

Furthermore the springs used in the model, might have absorbed the energy which comes due to seismic excitation.

Last but not least, the frictional pendulums on the abutments, play a significant role on reducing the energy due to seismic excitation.

The results of the analyses show that, under medium dense sand conditions, multiple column piers rotate more than hammerhead piers and footing vertical displacement of multiple column is higher than the footing vertical displacement of hammerhead.

REFERENCES

1. AASHTO LRFD Bridge Design Specifications. (2014). Washington.

2. Anastasopoulos, I., Gelagoti, F., Kourkoulis, R., & Gazetas, G. (2011). Simplified Constitutive Model for Simulation of Cyclic Response of Shallow Foundations: Validation against Laboratory Tests. Journal of Geotechnical and Geoenvironmental Engineering, 137(12), 1154-1168. doi:10.1061/(asce)gt.1943-5606.0000534

3. Anastasopoulos, I., Kourkoulis, R., Gelagoti, F., & Papadopoulos, E. (2012). Rocking response of SDOF systems on shallow improved sand: An experimental study. Soil Dynamics and Earthquake Engineering, 40, 15-33. doi:10.1016/j.soildyn.2012.04.006

4. Deng, L., Kutter, B. L., & Kunnath, S. K. (2012). Centrifuge Modeling of Bridge Systems Designed for Rocking Foundations. Journal of Geotechnical and Geoenvironmental Engineering, 138(3), 335-344. doi:10.1061/(asce)gt.1943-5606.0000605

5. Gajan, S., & Kutter, B. L. (2008). Effect of Critical Contact Area Ratio on Moment Capacity of Rocking Shallow Footings. Geotechnical Earthquake Engineering and Soil Dynamics IV. doi:10.1061/40975(318)133

6. Gajan, S., & Kutter, B. L. (2009). Contact Interface Model for Shallow Foundations Subjected to Combined Cyclic Loading. Journal of Geotechnical and Geoenvironmental Engineering,135(3), 407-419. doi:10.1061/(asce)1090-0241(2009)135:3(407)

7. Gajan, S., & Kutter, B. L. (2009). Effects of Moment-to-Shear Ratio on Combined Cyclic Load-Displacement Behavior of Shallow Foundations

from Centrifuge Experiments. Journal of Geotechnical and Geoenvironmental Engineering, 135(8), 1044-1055.

8. Gajan, S., Hutchinson, T., Kutter, B., Raychowdhury, P., Ugalde, J., & Stewart, J. (2008). Numerical models for analysis and performance-based design of shallow foundations subjected to seismic loading. Berkeley, CA: Pacific Earthquake Engineering Research Center.

9. Gajan, S., Kutter, B. L., Phalen, J. D., Hutchinson, T. C., & Martin, G. R. (2005). Centrifuge modeling of load-deformation behavior of rocking shallow foundations. Soil Dynamics and Earthquake Engineering,25(7-10), 773-783. doi:10.1016/j.soildyn.2004.11.019

10. Gajan, S., Kutter, B. L., Phalen, J. D., Hutchinson, T. C., & Martin, G. R. (2005). Centrifuge modeling of load-deformation behavior of rocking shallow foundations. Soil Dynamics and Earthquake Engineering, 25(7-10), 773-783. doi:10.1016/j.soildyn.2004.11.019

11. Gajan, S., Kutter, B., & Thomas, J. (2005). Physical and numerical modeling of cyclic moment-rotation behavior of shallow foundations.

12. Harden, C. W., Hutchinson, T., Martin, G. R., and Kutter, B. L., 2005, Numerical modeling of the nonlinear cyclic response of shallow foundations, Report No. PEER- 2005/04, Pacific Earthquake Engineering Research Center, University of California, Berkeley.

13. Kausel, E. (2010). Early history of soil–structure interaction. Soil Dynamics and Earthquake Engineering, 30(9), 822-832. doi:10.1016/j.soildyn.2009.11.001

14. Kim, Y., & Roesset, J. M. (2004). Effect of Nonlinear Soil Behavior on Inelastic Seismic Response of a Structure. International Journal of Geomechanics, 4(2), 104-114. doi:10.1061/(asce)1532-3641(2004)4:2(104)

15. Kokkali, P., Abdoun, T., & Anastasopoulos, I. (2015). Centrifuge Modeling of Rocking Foundations on Improved Soil. Journal of Geotechnical and Geoenvironmental Engineering,141(10), 04015041. doi:10.1061/(asce)gt.1943-5606.0001315

16. Mylonakis, G., Nikolaou, S., & Gazetas, G. (2006). Footings under seismic loading: Analysis and design issues with emphasis on bridge foundations. Soil Dynamics and Earthquake Engineering, 26(9), 824-853. doi:10.1016/j.soildyn.2005.12.005

17. Negro, P., Paolucci, R., Pedretti, S., & Faccioli, E. (2000). Large-scale soil-structure interaction experiments on sand under cyclic loading.

18. Raychowdhury, P., & Hutchinson, T. (2008). Nonlinear Material Models for Winkler-Based Shallow Foundation Response Evaluation. GeoCongress 2008. doi:10.1061/40972(311)85

19. Saadeghvaziri, M., Yazdani-Motlagh, A., & Rashidi, S. (2000). Effects of soil–structure interaction on longitudinal seismic response of MSSS bridges. Soil Dynamics and Earthquake Engineering, 20(1-4), 231-242. doi:10.1016/s0267-7261(00)00056-7

20. Salgado, R. (2003). The Engineering of Foundations.

21. Seismic Design of Highway Bridge Foundations (Vol. 2). (1986). McLean, Virginia: US Department of Transportation.

22. Shirato, M., Kouno, T., Asai, R., Nakatani, S., Fukui, J., & Paolucci, R. (2008). Large-Scale Experiments On Nonlinear Behavior Of Shallow Foundations Subjected To Strong Earthquakes. Soils And Foundations, 48(5), 673-692. doi:10.3208/sandf.48.673

23. Shirato, M., Yoshinori, N., & Ryuichi, A. (2005). Experimental study on the residual displacement of shallow foundations subjected to cyclic loads.

24. Ugalde, J., Kutter, B., Jeremic, B., & Gajan, S. (2007). Centrifuge modelling of rocking behavior of bridges on shallow foundations.

25. Yücemen, S., & Fırat, F. K. (2014). Determination of New Load and Resistance Factors for Reinforced Concrete Structural Members.